Multifrequency observations of extended radio galaxies V - 3C 31, 3C 33.1, 3C 35, 3C 66B, 3C 129, 3C 130, 3C 223, 3C 310, 3C 390.3 and 4C 48.29

Breugel, W.J.M. van; Jagers, W.

ASTRONOMY & ASTROPHYSICS
SUPPLEMENT SERIES

AUGUST 1982, PAGE 529

Astron. Astrophys. Suppl. Ser. **49**, 529-559 (1982)

Multifrequency observations of extended radio galaxies V : 3C 31, 3C 33.1, 3C 35, 3C 66B, 3C 129, 3C 130, 3C 223, 3C 310, 3C 390.3 and 4C 48.29

W. van Breugel ([1]) and W. Jägers ([2])

([1]) Kitt Peak National Observatory (*), P.O. Box 26732, Tucson, Arizona 85726, U.S.A.
([2]) Leiden Observatory, P.O. Box 9513, 2300 RA Leiden, The Netherlands

Received November 23, 1981, accepted February 16, 1982

Summary. — Total intensity and polarization maps obtained at several wavelengths with the WSRT, are presented for 10 extended radio galaxies. The sources were selected from the 3C survey such that their largest angular extent was $\gtrsim 200''$ and their declination $\gtrsim 25°$. 4C 48.29, a large source with peculiar morphology, was also included. The multifrequency comparison of the data will be given elsewhere.

Key words : radio galaxies — radio jets — polarization.

1. **Introduction.** — To improve our knowledge of the physical conditions in radio galaxies a sample of 3C radio sources of large angular size has been observed in total and polarized intensity at several wavelengths with the Westerbork Synthesis Radio Telescope (WSRT). In order to have at least two resolution elements at the largest wavelength (49 cm) the sources were selected such that their largest angular size was $\gtrsim 200''$ and their declination $\gtrsim 25°$. Some additional sources with radio jets or peculiar morphology were also included. For convenience the complete list of sources that was selected initially is given in table I. Column 1 gives the name of the source, column 2 the classification of the structural type adopting the morphological scheme of Miley (1980), crosses in columns 3, 4 and 5 indicate at which wavelength a source was observed and column 6 gives a reference where the most recent data of the source are discussed. Some of the sources were not observed because these have been discussed in detail by other authors, other sources were not included because the observations were of poor quality. The sample includes objects of every morphological class although our selection criteria discriminate in favour of nearby sources of relatively low radio luminosities. Such sources are known to have complex morphologies (Fanaroff and Riley, 1974) and several of these were found to have radio jets or other fine structure.

For several of the sources a detailed multifrequency comparison has already been made (see Table I). An analysis of the remaining sources will be given elsewhere. Similar multifrequency studies generally of more powerful sources have been made by Burch (1979a, 1979b), Högbom (1979) and Laing (1980).

(*) Work completed while at Leiden Observatory.

2. **The observations.** — The observational parameters are given in tables II and III. During the course of this research several major changes have been made to the WSRT. Between January 1978 and August 1979 two additional movable telescopes came into operation increasing the number of interferometers of the 1.5 km array from 20 to 40. The backends were changed (January 1978) such that the incoming signal was digitally recorded and new cooled frontends were put into operation : at 6 cm (50 K (4 movable telescopes) + 130 K (10 fixed telescopes)), at 21 cm (90 K) and at 49 cm (325 K). Furthermore the bandwidth available for continuum observations was increased from 4 MHz to 10 MHz.

The resulting increase in sensitivity was most profitable at 6 cm and enabled the mapping at full resolution of the polarization distribution to much fainter levels. In table II, column 8 the rms noise at the field centre is given. These values were derived from circular polarization maps, assuming no contribution from the source itself. Since the sources that are studied here are extended and mostly weak, this is a safe assumption (see for example Weiler and Raimond, 1977). These values are only relevant for maps which are noise limited. This was mostly the case for the polarization maps. For various reasons, i.e. unstable temperature control in the receivers (at 6 cm) and ionospheric disturbances (at 49 cm) the 6 cm and 49 cm were limited in dynamic range and an estimate of the peak residual intensity in the map which was left after « cleaning » (Högbom, 1974) is given in column 9.

Except for the use of updated and new reduction software developed by the SRZM Reduction Group (e.g. Harten, 1978) the data was reduced in a standard way (Weiler, 1973 ; Högbom and Brouw, 1974). At 49 cm ionospheric corrections were applied to the polarization position angles (Strom, 1972). Although due to increasing solar activity, ionospheric disturbances were larger at the

time of observations than in previous years, they were limited to relatively short periods of time. A check on the integrated polarization position angles was possible for 3C 33.1 and 3C 390.3 and in both cases they agreed within the errors with the values found by Kronberg and Conway (1970), after including the correction given by Conway *et al.* (1972), and Strom (1973) respectively. Unfortunately however a possible systematic error of 10°-20° *may* exist at 49 cm in the other sources (3C 35, 3C 310, 4C 40.29), for which no independent checks are available, due to a small bug in the ionospheric Faraday corrections program applied to observations until end 1980 (Spoelstra, priv. comm.).

The integrated parameters for all sources are listed in table IV. The 6 cm parameters were obtained by integrating over the appropriate areas in the maps after a primary beam correction was applied. At 21 cm and 49 cm the parameters were derived from the visibility data at the shortest baselines. The integrated values generally agree reasonably well with single dish values reported in the literature (e.g. Kellermann *et al.,* 1969 ; see Tabara and Inoue, 1980 for a compilation of polarization data). In a few of the very extended sources some of the flux apparently is missing due to the lack of very short interferometer spacings.

3. **The maps.** — The maps are shown in figures 1-60. Polarization position angles (ϕ) are overlayed on contour maps of the total intensity (I). For display reasons the lengths of the line segments of ϕ are of equal length and the polarized intensity (P) is given as a separate contour map. Where no separate P-contour map is shown the length of the line segments is proportional to the polarized intensity. Brightness contour levels are in mJy/beam. Crosses indicate galaxy positions with a typical uncertainty of $\sim 0.5''$ in both right ascension and declination and stars in the 6 cm maps indicate the pointing position of the telescopes in cases where this is significantly different from the galaxy position.

None of the maps have been corrected for primary beam attenuation because the noise distribution would then be non-uniform across the map. However, these corrections are important at 6 cm for most of the sources, since the halfpower halfwidth (HPHW) of the primary beam at 6 cm is $\sim$ 5 arcmin. The WSRT primary beam attenuation as a function of radius has been taken from Willis and Miley (1979).

Instrumental polarization at the half power intensity point in the primary beam is $\lesssim$ 2 % at 6 cm (Weiler and Wilson, 1973 ; Strom priv. comm.) and $\lesssim$ 1 % at 21 cm (Weiler *et al.,* 1973). At 49 cm the primary beam is so large ($\sim$ 40 arcmin.) that its effect on the polarization can be neglected and the instrumental polarization which is dominated by instrumental gain and phase drifts is typically $\lesssim$ 0.5 %.

The percentage polarization distribution was determined after applying an average zero level correction for the total intensity maps when necessary (e.g. Miley *et al.,* 1975). This was never more than a few mJy/beam. The maps are presented as number/character maps except in a few cases where there were only two or three independent resolution elements. In those cases the percentages polarization are given in the description of the source. The percentage polarization in the maps was binned with b = 1 %, 2.5 % or 5 % intervals indicated in the left corners. The key relating the numbers/characters to these bins is : < = (< b), 1 = (1b to 2b), ..., 9 = (9b to 10b), A = (10b to 11b), ..., F = (15b to 16b) > = (> 16b). An independent resolution element contains 2.5 × 2.5 pixels. Note that for ease of display the declination scale in the printed maps is compressed with respect to that in right ascension to give equal numbers of pixels per beam in both directions. The lowest contours from the total intensity maps given in the figure captions are drawn to delineate the source structure and a star indicates the position of the radio core. The right ascension is expressed in degrees. The maps show in general an increase of the percentage polarization along the boundaries of a source. This may be partially due to increased instrumental polarization at gradients of the synthesized beam.

Using maps of the unresolved, unpolarized calibrator 3C 147 we found that the percentage polarization at the half power points was at most $\sim$ 1 % at 6 cm and 21 cm. This may serve as an indication for the possible systematic errors encountered at steep gradients such as at the extreme edges of sources.

In table V the radio core positions and flux densities at 6 cm are listed (columns 2, 3, 4) together with the visual magnitudes of the galaxies and their redshifts (columns 5, 6), the luminosity distances derived assuming H_0 = 100 km s^{-1} Mpc^{-1} and q_0 = 0.5 (column 7) and the angular to linear size conversion ratios using the angular size distances (column 8). References for the redshifts are given in column 9. For several sources the radio cores were not detected previously. All proposed optical identifications have been confirmed.

4. **Notes on the sources.** — 3C 31. — This source is identified with NGC 383 (Humason *et al.,* 1956), a member of the chain of galaxies Arp 331 (Arp, 1966). The galaxy has a dust lane and an optical jet coincident with the bright base of the northern radio jet (Butcher *et al.,* 1980). The total angular extent of the source is $\sim$ 30 arcmin. and its two opposite radio jets have been studied extensively by Burch (1977b, 1979c), who included a comparison of 11 cm and 21 cm polarization data. Very high resolution ($\sim 1.4''$) total intensity and polarization maps at 6 cm have been made by Fomalont *et al.* (1980) with the VLA. The present WSRT 6 cm observations, at a much lower resolution ($\sim 7'' \times 7''$ cosec δ show polarized emission over a larger part of the source than the convolved ($\sim 4.5''$) 6 cm map by Fomalont *et al.*

Polarized emission is now detected along the boundaries of the southern jet and also beyond the first bends of both jets. The percentage polarization measured along the centre lines of the jets is relatively low at our resolution : 5 %, increasing to 20 % in the southern jet until it drops rapidly below 10 % at 60″ from the core (see Fig. a). The higher resolution polarization maps by Fomalont *et al.* show oscillations in the percentage polarization in particular in the southern jet. These oscillations, which seem to occur around a mean value

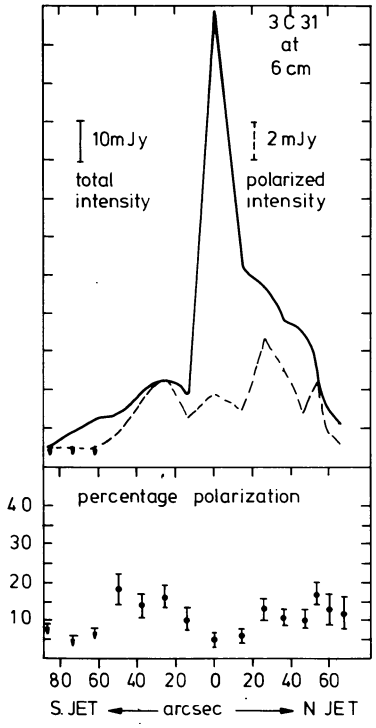

FIGURE a. — Total and polarized intensity and percentage polarization along the ridge line of the jets in 3C 31.

which steadily decreases southwards along the jet, are smoothed within our larger observing beam. At the place where the polarized flux density and the percentage polarization in the center of the jet become low, the flux density and the percentage at the boundaries increase (up to ~ 40 %). A high percentage polarization is found at all places where the jets bend. At these bends the magnetic field is parallel to the jet direction (van Breugel, 1982). These results suggest that shearing at the interface of the jets and a surrounding medium may enhance and order the magnetic field.

3C 33.1. — We detect a weak radio core in this source (Table IV) which confirms its identification with a 19.5-20th magnitude double galaxy suggested by Longair and Gunn (1975). A previous 21 cm map made with the WSRT was published by Högbom and Carlsson (1974) and a 2″ resolution map at 6 cm of the northern hot spot was published by Jenkins *et al.* (1977). The radio galaxy, at low resolution described as a quadrupole or double-double (see 21 cm map), is well resolved at 6 cm except for its hot spots and a narrow elongated bridge or jet located halfway between the core and the southern hot spot. The structure of 3C 33.1 resembles that of 3C 219, a three times more luminous double source with a strong jet (e.g. Perley *et al.*, 1980). Interpreting the narrow structure in the southern lobe as a jet, the gap between the core and the jet (47 arcsec, 90 kpc) is much larger than that in 3C 219 (5 arcsec, 17 kpc). It shows that the terms « jet » or « bridge » are perhaps only a semantic distinction. The low brightness structure perpendicular to the major axis of the southern lobe is uncertain and could be a cleaning artifact, since at the time of the observations the dynamic range was relatively poor. The core, the northern hot spot and the brightest peak in the jet are aligned to within a few degrees in a position angle of 43.5°. The jet itself however points neither to the core nor to the southern hot spot. Also misalinged are the « tail » at the northern hot spot and the core. The source has a slight S-shape and the misalignments may be caused by changes in the ejection direction for example due to precession or to orbital motion of the parent galaxy around its companion.

The polarized intensity is most prominent along the jet and at the northern hot spot. In the jet the percentage polarization at 6 cm is 30-40 %, in the northern hot spot ~ 5 % and 10-15 % in the tailed extension. In the diffuse lobes the percentage can be as high as 50-60 % but here the errors are large.

The foreground rotation in the direction of 3C 33.1 (Galactic coordinates $\ell_{II} = 124.3°$, $b_{II} = 10.4°$) is probably between 0 rad m^{-2} and − 30 rad^{-2} (Simard-Normandin and Kronberg, 1979) so that the magnetic field in 3C 33.1 is generally parallel to the jet direction, similar to that in 3C 219.

At 21 cm a strong polarized ridge is observed in the south-eastern part of the southern lobe. This ridge appears to be at least partially associated with the jet. The percentage polarization at the position of the jet is 10-15 % at 21 cm. In the northern lobe the polarized intensity shows a Z-shape, linking the northern hot spot with the core. The percentage polarization is lowest at the hot spot ($\lesssim$ 2.5 %), the highest values are found along the outer boundaries.

3C 35. — Of this large source (11.2 arcmin., 590 kpc) only crude low resolution maps existed, made at 408 MHz and 1.4 GHz (Mackay, 1969), since it is rather weak (~ 10 Jy at 178 MHz). Because of its large extent the two lobes were mapped separately at 6 cm. These maps are shown combined in figure 12. The two different pointing centres are indicated by stars.

We detect a weak radio core (Table V) which coincides with the nucleus of a 14.5 magnitude galaxy and confirms the identification proposed by Burbidge and Strittmatter (1972). Both lobes are completely resolved and structure at the two lowest contour levels is noise limited. The « hot spot » in the southern lobe may be double with each of the components being resolved. The maximum intensities are ~ 1.5 mJy/beam and ~ 3 mJy/beam. The hot spot in the northern lobe is nearly square (~ 60 kpc × 60 kpc) and has a ridge at position angle 36° connected with a knot (~ 8 mJy/beam) at the sharp north-eastern boundary. Beyond this boundary there is weak emission which is also present in the 21 cm map (Fig. 16). At full resolution the only polarized emission was detected from this knot : 32 % ± 5 % at the boundary and 25 % ± 5 % south-west of this.

The 6 cm maps have been convolved to 23″ × 23″ cosec δ resolution to obtain better sensitivity for low brightness structure (Figs. 14 and 15). We detected polarization in the northern lobe with percentages of 23 ± 3 % and 15 ± 5 % at locations a and b, and in the southern lobe of 23 ± 5 %, 15 ± 5 % and 50 ± 10 % at locations c, d and e.

The 21 cm maps show the full extent of the source which has a nearly rectangular morphology and a bridge in the middle. The curiously shaped hot spots have their largest intensity gradients (projected ?) inside the source. The ridge in the northern hot spot seen at 6 cm full resolution can be traced also in the 21 cm map. Polarization is detected along the bridge, the boundaries and near the hot spots. The percentage polarization in the bridge is highest near the core, decreasing in the direction of the hot spots. The highest percentage polarization in both lobes is found along the eastern boundary. Not much polarization is found west of the southern hot spot. This is probably due to beam smearing.

The 49 cm maps are shown in figures 19, 20, 21. Here the flat spectrum core is not detected. The source is appreciably polarized also at this wavelength. The spatial distribution of the brightness and polarization follows the same trend as at 21 cm.

3C 66B. — This well known complex source is identified with a 12.9 magnitude elliptical galaxy situated at the edge of the cluster A 347. The galaxy has two nearby companions and an optical jet coincident with the bright base of a strong radio jet, similar to that in 3C 31 (Butcher *et al.*, 1980). 3C 66B has been studied in total intensity at several radio wavelengths by Northover, 1973. Previously 21 cm total intensity and polarization observations have been made by Miley and van der Laan (1973). Here we present 6 cm, and new more sensitive 21 cm and 49 cm observations of this source. The 21 cm and 49 cm observations were kindly provided by Drs. D. E. Harris, R. G. Strom and G. K. Miley. Polarization was detected at 6 cm and 21 cm. At 49 cm interference precluded the construction of reliable polarization maps.

The 6 cm observations were not without problems because of the unrelated strong background source 3C 66A (see at the end of this section) and spurious grating rings remained after the map had been cleaned to a residual level of ~ 4 mJy/beam. An attempt was made to self-calibrate the data using the (slightly resolved) source 3C 66A but this did not improve greatly the dynamic range of the map. Nevertheless, at brightness levels $\gtrsim$ 4 mJy/beam the source is not severely affected by these problems. Note that the contour levels shown in figure 22 increase logarithmically. The polarized intensity was only slightly affected by 3C 66A at a level of $\lesssim$ 0.5 mJy/beam.

The overall appearance of the source ressembles that of a trumpet with the expanding jet appearing to open rather abruptly at its end. Along the ridge line of the jet the percentage polarization is < 10 % until ~ 80 arcs (~ 24 kpc) from the parent galaxy and then increases quickly to ~ 60 % at the end (Fig. b). 3C 66B has a weak radio counterjet with a maximum intensity of 32 mJy/beam. No significant polarization is detected from this counterjet until it merges with the extended western radio lobe. In this lobe there are slight brightness enhancements which appear to be surrounded by polarized emission at the extrapolated end of the counterjet. The percentage polarization is the highest along the boundaries of the lobes.

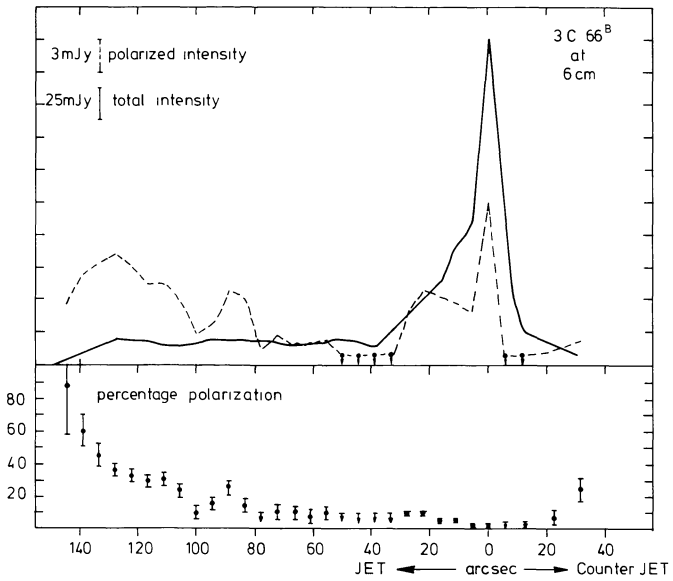

FIGURE b. — Total and polarized intensity and percentage polarization along the ridge line of the jets in 3C 66B.

Compared with the previous 21 cm observations by Miley and van der Laan (1973) our new 21 cm observations show that the low brightness lobe of the source is ~ 2 arcmin. larger, giving a total extent for the source of ~ 10.3 arcmin. (~ 190 kpc). The overall appearance is that of a head tail source seen partly head- or tail-on.

Part of the eastern lobe may be seen mostly in projection. The morphology of the source may have been complicated further by orbital motion because there are two nearby companion galaxies (Butcher *et al.*, 1980). Dynamic range in the 21 cm observations was good (~ 25 dB) but still a spurious grating ring(~ 5 mJy/beam) remained from 3C 66A. Although confused by the grating ring, the upward bending at the end of the eastern lobe of 3C 66B is real (compare 49 cm map figure 28).

Using the slightly resolved source 3C 66A as a phase reference our 21 cm polarized intensity map was slightly improved and a spurious grating ring removed. The accuracy of these polarization measurements is limited to ~ 0.4 % of the maximum intensity of the brightness map. In the eastern lobe in 3C 66B the percentage polarization is rather low (< 4 %). Along the boundaries much higher values are found.

The 49 cm map essentially confirms the structure observed at 21 cm i.e. the source is not larger and the upward bending of the source close to its eastern edge seen at 21 cm is also apparent.

Positions and flux densities of the two sources in the contour maps unrelated to 3C 66B.

Name	RA (1950) H M S	DEC (1950) D M S	Wave-length (cm)	Flux density (mJy)
3C 66A	02 19 29.91 ± 0.05	42 48 30.2 ± 0.3	21	1900 ± 24*
			49	3391 ± 38
0219+428	02 19 46.83 ± 0.05	42 50 01.7 ± 0.4	21	47.6 ± 0.8
			49	90 ± 8

* : peak intensity since the source is resolved.

3C 66A is polarized at 21 cm : 2.0 ± 0.5 %, position angle 50° ± 10° at the centre. There is a tendency of the percentage polarization to be larger at the edges of 3C 66A but this is rather uncertain due to the very large intensity gradients.

3C 129. — This very long narrow tailed source (~ 30 arcmin., ~ 520 kpc) is identified with a 19.4 magnitude galaxy (Spinrad, 1975) situated in a nearly obscured area of the galactic plane. Its Galactic coordinates are ℓ_{II} = 160.3°, b_{II} = 0.1°. Its morphology is thought to be mainly produced by motion of the parent galaxy through an intracluster medium (Miley *et al.,* 1972 ; Miley, 1973). 3C 129 has been studied by many authors, most recently by Owen *et al.* (1979), Downes (1979) and Perley and Erickson (1979).

Because of the steepening of the spectrum along the tail, previously only the head of the source was seen at short wavelengths. The increased sensitivity of the WSRT allowed to map a much larger part of the source at 6 cm (Fig. 29). The pointing of the telescopes was centered in the tail at approximately 7.5 arcmin. from the head. That part of the source is far beyond the half power radius of the primary beam (at ~ 5 arcmin.). This means that the attenuation is large and not accurately known and that instrumental polarization may be important. To check on this were therefore observed the head of 3C 129 in a separate observing run using 6 short (~ 30 min.) observations which were well spread in hour angles. Comparing maps from these observations with the full synthesis maps centered at the tail we conclude that 1) instrumental polarization is negligible and 2) the average attenuation factor for the head is 2.7 ± 0.6. Within approximately one beamsize from the fringe stopping centre in the tail (indicated by a star), the source structure may be distorted at a level of ~ 1 mJy/beam due to a small instrumental problem occurring at the time of the observations.

Note that the 6 cm maps have not been corrected for primary beam attenuation ([1]). From the observations centered at the head we infer a flux density of 34 ± 4 mJy for the radio core at RA (1950) = $04^h45'31.92'' \pm 0.05''$ and DEC (1950) = $44°55'29.0'' \pm 0.3''$. This core is slightly extended in northward direction and high resolution observations with the VLA have shown that it contains a one-sided jet (Owen *et al.,* 1979). Departing from this core are two parallel, expanding streamers or jets with equivalent wiggles. At the point where the expansion stops the structure becomes more complicated. Along the tail, weak streamers are found. Note that low brightness structure with an angular scale size of ≳ 4 arcmin. is not present in the map because of missing short spacings and also because much of the resolved structure will remain below the detection level at full resolution. The percentage polarization is 5-10 % at the beginning of the head in the two jets rising to ~ 70 % far out along the tail. In the head the percentage polarization is highest near the boundaries of the jets.

([1]) Note : Also the total intensity contour map of previous 6 cm observations of 3C 129 (van Breugel and Miley, 1977) was not corrected for primary beam attenuation, contrary to what was stated.

The 49 cm observations (Fig. 34) were kindly provided by Dr. D. E. Harris and Dr. G. K. Miley. The map shows that the source is still somewhat larger than observed at 21 cm (Miley and van der Laan, 1973). At RA (1950) $04^h44'15''$, DEC (1950) = $44°53'00''$ the tail is broader. This is approximately at the place where Perley and Erickson (1979) find a brightness enhancement at very low frequencies. For the polarization a 3σ upper limit of ~ 1.5 % can be set for both head and tail.

A weak unresolved background source is apparent at RA (1950) = $04^h44'45.10'' \pm 0.07''$ and DEC (1950) = $45°00'19.4'' \pm 0.9''$. The flux density is 3.4 ± 0.4 mJy at 6 cm and 5.0 ± 0.5 mJy at 21 cm.

3C 130. — This wide-angled tail source also lies in an obscured part near the Galactic plane (l_{II} = 155.4°, b_{II} = 5.1°). It is relatively weak (15.5 Jy at 178 MHz) and has previously been mapped with the WSRT at 21 cm by Högbom and Carlsson (1974).

We detect the radio core at 6 cm (Table V) which confirms the identification with a 16.5 magnitude (reddened) galaxy at a redshift of z = 0.1090 (Smith *et al.,* 1976). On the Palomar Sky Survey plates several galaxies are found of similar magnitude some of which constitute a chain. Their positions are plotted as crosses in the figures. The 6 cm total intensity map was distorted due to bad dynamic range caused by temperature variations in the receivers at the time of the observations. This did not affect the much weaker polarized intensities. The polarization position angles in the south-western tail show variations on the scale size of a resolution element while the variation is much smoother in the north-eastern tail. The percentage polarization is on average higher in the south-western tail.

The new 21 cm and 49 cm WSRT observations show that the extent of the source is ~ 9.4 arcmin. (~ 750 kpc) i.e. much larger than previously could be inferred from the 21 cm map by Högbom and Carlsson (1974). The polarization distribution is rather asymmetric. The polarized intensity is much higher in the north-eastern tail than in the south-western tail which is nearly entirely depolarized (≲ 5 % polarization) except near the end where the tail curves.

3C 223. — Previous WSRT maps of this source made at 6 cm and 21 cm have been published by Högbom (1979) and Högbom and Carlsson (1974). The new observations presented here, made with better sensitivity, confirm the features shown by those maps and show weaker structure (at 6 cm) and have better signal-to-noise in the polarization maps. The hot spots have been mapped at 6 cm with 2″ resolution using the Cambridge 5 km telescope (Riley and Pooley, 1975).

At 6 cm we detect the core (Table V) ~ 3 arcsec. north of the position at which the proposed identification is located (a 17.1 galaxy in a small group ; Riley and Pooley, 1975). The discrepancy could be due to a blending in our observations between the core emission and that of the northern bridge. The southern lobe of 3C 223 resembles that of the northern lobe in 3C 219 (Perley *et al.,* 1980) in that the hot spot seems embedded in the lobe and a somewhat fainter protrusion is seen at the end. The percentage polarization is the lowest at the hot spots and the highest along the boundaries.

3C 310. — This wide double source is identified with a 15.2 magnitude galaxy which has two nearby companions. A comparison of previous 6 cm and 21 cm observations with the WSRT is discussed by van Breugel (1980, I).

The observations presented here are of superior sensitivity but inferior dynamic range. They are useful for investigation of the brightness structure far from the core ($\gtrsim$ 1 arcmin.) and of the polarization structure. The curved structure embedded in the southern lobe and faint brightness enhancements (« knots ») in the outer regions of both lobes inferred to exist in the previous observations, are confirmed. Note also the « holes » in the centre of the southern lobe and the curved « flux tube » north-west of the source. Because there are so many resolution elements in this large source, the clean procedure has not completely removed the negative bowl due to the missing short spacings (e.g. Miley *et al.*, 1975). The brightness levels of the extended structure are therefore subject to relatively small (1-2 mJy/beam) offsets.

Polarized intensity in 3C 310 is found at the boundaries of the hot spots, around the hole and along the flux tube. The observed percentage polarizations varied from as low as $\lesssim$ 10 % in the northern hot spot to as high as 70 % at the north-western boundary of the source.

At the latter position polarized emission (9 ± 5 %) was also detected at 49 cm. The polarization position angles at 6 cm, 21 cm and 49 cm are almost the same (compare with Miley and van der Laan, 1973 (21 cm) and van Breugel, 1980, I (convolved 6 cm)). Thus presumably the foreground rotation measure can be neglected and the magnetic field structure of 3C 310 can therefore be derived by rotating the polarization position angles at 6 cm through 90°.

Although 3C 310 has a steep spectrum at high frequencies (Véron *et al.*, 1974 ; van Breugel, 1980, I) the source is not observed to be significantly larger at 49 cm.The 49 cm map is however limited by dynamic range due to ionospheric fluctuations.

3C 390.3. — This classic edge brightened double source is identified with a 14.5 magnitude (variable) N-type galaxy. It has recently been studied using the Cambridge 5 km telescope with ~ 2″ resolution at 6 cm by Hargrave and McEllin (1975) and compared with ~ 4″ resolution 11 cm observations by Laing (1980). 21 cm WSRT maps have been published by Högbom and Carlsson (1974) and Miley and van der Laan (1973).

The WSRT 6 cm map was severely dynamic range limited and at this wavelength we therefore report only the flux density of the core (see Table V).

The 49 cm map is shown in figure 52. In the northern lobe there is a significant amount of polarization increasing from ~ 2 % in the middle of the bridge to ~ 7 % near the hot spot. This contrasts with the southern lobe where the percentage polarization is $\lesssim$ 1 %, perhaps slightly larger along the boundaries. Compared with the maps at the other wavelengths mentioned above the polarization position angles are nearly the same at all wavelengths for the northern lobe but not for the southern lobe. For the latter the wavelength dependence of the polarization is presumably more complicated due to the much brighter hot spot.

4C 48.29. — This source has been partly mapped previously at 11 cm with the NRAO three element interferometer by Burns and Owen (1979). This map did not show the bright southern hot spot ~ 2.9 arcmin. south of the core (components C and D ; Fig. 54). The source is identified with a 16th magnitude elliptical galaxy member of a pair and its redshift (z = 0.052) has been measured by Miley and Osterbrock (1979).

From the 6 cm maps it appears that the brightest components of the hot spots are well aligned with the core. Of the two components of the southern hot spot the weaker (D) is the further away from the core. The boundaries of the resolved component D is polarized with a percentage of 15 ± 6 % and the bright component C with 8 ± 3 %.

The 21 cm map shows the peculiar large scale structure of the source. Note that some fainter emission exists beyond the northern hot spot. The percentage polarization is the lowest near the hot spots and the highest along the boundaries.

The 49 cm map confirms the structure seen in the 21 cm map and also significant polarization is found. The percentage polarization is on average the highest in the southern lobe.

The morphology of 4C 48.29 resembles that of 3C 315 (Högbom, 1979) and NGC 326 (Ekers *et al.*, 1978) and suggests that tidal interaction between the pair of galaxies has caused the nuclear source of the parent galaxy to precess. Swinging of the beam along the line of sight would then mean that the hot spots are seen projected onto the lobes.

Acknowledgements. — We thank the staff of the Westerbork Radio Telescope and the Reduction Group for their work on these observations, in particular Dr. T. A. Th. Spoelstra for the calibrations, Dr. R. G. Strom for applying the ionospheric Faraday corrections at 49 cm and K. W. C. Lugtenborg for his advice on job control handling of the batch programs. We are grateful to Dr. G. K. Miley and Prof. H. van der Laan for useful discussions and comments on the manuscript. W. Brokaar prepared the figures and the manuscript was typed by Petra Steehouwer.

The investigations were supported (in part) by the Netherlands Foundation for Astronomical Research (ASTRON). The Westerbork Synthesis Radio Telescope is operated by the Netherlands Foundation for Radio Astronomy (SRZM). Both Foundations are supported financially by the Netherlands Organization for the Advancement of Pure Research (Z.W.O.).

References

ARP, H. : 1966, Atlas of peculiar Galaxies. California Institute of Technology.
BREUGEL, W. J. M. VAN, MILEY, G. K. : 1977, *Nature* **265,** 315.
BREUGEL, W. J. M. VAN : 1980 (I), *Astron. Astrophys.* **81,** 265.
BREUGEL, W. J. M. VAN : 1980 (II), *Astron. Astrophys.* **81,** 275.
BREUGEL, W. J. M. VAN : 1980 (III), *Astron. Astrophys.* **88,** 248.
BREUGEL, W. J. M. VAN, WILLIS, A. G. : 1980 (IV), *Astron. Astrophys.* **96,** 332.
BREUGEL, W. J. M. VAN : 1982, *Astron. Astrophys.* (in press).
BURBIDGE, E. M., STRITTMATTER, P. A. : 1972, *Astrophys. J.* **172,** L37.
BURCH, S. F. : 1977a, *Mon. Not. Roy. Astron. Soc.* **180,** 623.
BURCH, S. F. : 1977b, *Mon. Not. Roy. Astron. Soc.* **181,** 599.
BURCH, S. F. : 1979a, *Mon. Not. Roy. Astron. Soc.* **186,** 293.
BURCH, S. F. : 1979b, *Mon. Not. Roy. Astron. Soc.* **186,** 519.
BURCH, S. F. : 1979c, *Mon. Not. Roy. Astron. Soc.* **187,** 187.
BURNS, J. O., OWEN, F. N. : 1979, *Astron. J.* **84,** 1478.
BUTCHER, H., BREUGEL, W. J. M. VAN, MILEY, G. K. : 1980, *Astrophys. J.* **235,** 749.
DOWNES, A. : 1979, *Mon. Not. Roy. Astron. Soc.* **190,** 261.
EKERS, R. D., FANTI, R., LARI, C., PARMA, P. : 1978, *Nature* **276,** 588.
FANAROFF, B. L., RILEY, J. M. : 1974, *Mon. Not. Roy. Astron. Soc.* **167,** 31P.
FOMALONT, E. B., BRIDLE, A. H., WILLIS, A. G., PERLEY, R. A. : 1980, *Astrophys. J.* **237,** 418.
HARGRAVE, P. J., MCELLIN, M. : 1975, *Mon. Not. Roy. Astron. Soc.* **173,** 37.
HARTEN, R. H. : 1978, Internal Technical Report ITR-153 of the Netherlands Foundation for Radio Astronomy.
HÖGBOM, J. A., CARLSSON, I. : 1974, *Astron. Astrophys.* **34,** 341.
HÖGBOM, J. A. : 1974, *Astron. Astrophys. Suppl. Ser.* **15,** 417.
HÖGBOM, J. A., BROUW, W. N. : 1974, *Astron. Astrophys.* **33,** 289.
HÖGBOM, J. A. : 1979, *Astron. Astrophys. Suppl. Ser.* **36,** 173.
HUMASON, M. L., MAYALL, N. U., SANDAGE, A. R. : 1956, *Astron. J.* **61,** 97.
JENKINS, C. J., POOLEY, G. G., RILEY, J. M. : 1977, *Mem. Roy. Astron. Soc.* **84,** 61.
KELLERMANN, K. I., PAULINY-TOTH, I. I. K., WILLIAMS, P. J. S. : 1969, *Astrophys. J.* **157,** 1.
KRONBERG, P. P., CONWAY, R. G. : 1970, *Mon. Not. Roy. Astron. Soc.* **147,** 149.
LAING, R. A. : 1981, *Mon. Not. Roy. Astron. Soc.* **195,** 261.
LONGAIR, M. S., GUNN, J. E. : 1975, *Mon. Not. Roy. Astron. Soc.* **170,** 121.
MACKAY, C. D. : 1969, *Mon. Not. Roy. Astron. Soc.* **145,** 31.
MALTBY, P., MATHEWS, T. A., MOFFET, A. T. : 1963, *Astrophys. J.* **137,** 153.
MILEY, G. K., PEROLA, G. C., KRUIT, P. C. VAN DER, LAAN, H. VAN DER : : 1972, *Nature* **237,** 269.
MILEY, G. K. : 1973, *Astron. Astrophys.* **26,** 413.
MILEY, G. K. : LAAN, H. VAN DER : 1973, *Astron. Astrophys.* **28,** 359.
MILEY, G. K., WELLINGTON, K. J., LAAN, H. VAN DER : 1975, *Astron. Astrophys.* **38,** 381.
MILEY, G. K., OSTERBROCK, D. E. : 1979, *Publ. Astron. Soc. Pacific* **91,** 257.
MILEY, G. K. . 1980, *Ann. Rev. Astron. Astrophys.* **18,** 165 (in press).
NORTHOVER, K. J. E. : 1973, *Mon. Not. Roy. Astron. Soc.* **165,** 369.
OSTERBROCK, D. E., KOSKI, A. T., PHILLIPS, M. M. : 1975, *Astrophys. J.* **197,** L41.
OWEN, F. N., BURNS, J. O., RUDNICK, L., GREISEN, E. W. : 1979, *Astrophys. J.* **229,** L59.
PERLEY, R. A., ERICKSON, W. C. : 1979, *Astrophys. J. Suppl.* **41,** 131.
PERLEY, R. A., WILLIS, A. G., SCOTT, J. S. : 1979, *Nature* **281,** 437.
PERLEY, R. A., BRIDLE, A. H., WILLIS, A. G., FOMALONT, E. B. : 1980, *Astron. J.* **85,** 499.
RILEY, J. M., POOLEY, G. G. : 1975, *Mem. Roy. Astron. Soc.* **80,** 105.
SANDAGE, A. : 1978, *Astron. J.* **83,** 904.
SARGENT, W. L. W. : 1977, *Astrophys. J.* **212,** L105.
SIMARD-NORMANDIN, M., KRONBERG, P. P. : 1979, *Nature* **279,** 115.
SMITH, H. E., SPINRAD, H., SMITH E. O. : 1976, *Publ. Astron. Soc. Pacific* **88,** 621.
SPINRAD, H. : 1975, *Astrophys. J.* **199,** L1.
STROM, R. G. : 1972, Internal Technical Report ITR-99 of the Netherlands Foundation for Radio Astronomy.
STROM, R. G. : 1973, *Astron. Astrophys.* **25,** 303.
STROM, R. G., WILLIS, A. G. : 1980, *Astron. Astrophys.* **85,** 36.
TABARA, H., INOUE, M. : 1980, *Astron. Astrophys. Suppl. Ser.* **39,** 379.
VÉRON, M. P., VÉRON, P., WITZEL, A. : 1974, *Astron. Astrophys. Suppl. Ser.* **13,** 1.
WEILER, K. W. : 1973, *Astron. Astrophys.* **26,** 403.
WEILER, K. W., WILSON, A. S. : 1973, Technical Note TN-136 of the Netherlands Foundation for Radio Astronomy.
WEILER, K. W., SOMEREN GREVE, H. VAN, PIERSMA, Th. R. : 1973, Internal Technical Report ITR-117 of the Netherlands Foundation for Radio Astronomy.
WEILER, K. W., RAIMOND, E. : 1977, *Astron. Astrophys.* **54,** 965.
WILLIS, A. G., STROM, R. G. : 1978, *Astron. Astrophys.* **62,** 375.
WILLIS, A. G., MILEY, G. K. : 1979, *Astron. Astrophys. Suppl. Ser.* **37,** 397.

TABLE I.

Source	Morphological[+] classification	6 cm	21 cm	49 cm	Recent references for other maps
3C 31	NedD	x	-	-	Burch, 1977[a], 1979[c] Fomalont et al., 1980
3C 33.1	NebD	x	x	x	Jenkins et al., 1977
3C 35	NebD	x	x	x	Mackay, 1969
3C 66[B]	C	x	x	x	Northover, 1973
3C 83.1	NT	-	-	-	Miley et al., 1975
3C 111	NebD	-	-	-	Högbom, 1979
3C 129	NT	x	x	x	Owen et al., 1979; Downes, 1979 Perley and Erickson, 1979
3C 130	WT	x	x	x	Högbom and Carlsson, 1974
3C 223	NebD	x	x	-	Högbom, 1979
3C 236	NebD	-	-	-	Strom and Willis, 1980
3C 310	WD	x	x	x	van Breugel, 1980 (I)
3C 326	NebD	-	-	-	Willis and Strom, 1978
3C 390.3	NebD	-	-	x	Laing, 1980
3C 402	NedD	-	-	-	Miley and van der Laan, 1973
3C 449	NedD	-	-	-	Perley et al., 1979
3C 452	NebD	-	-	-	Burch, 1977[a]
3C 465	WT	x	x	x	van Breugel, 1980 (III)
B 0844+31	NedD	x	x	x	van Breugel, 1980 (II)
4C 48.29	C	x	x	x	Burns and Owen, 1979
4CT 74.17.1	NedD	x	x	x	van Breugel and Willis, 1980 (IV)

[+]Following Miley (1980):

NebD = narrow edge brightened double
NedD = narrow edge darkened double
WD = wide double
NT = narrow tailed
WT = wide tailed
C = complex

TABLE II. — *Observational parameters.*

1 Source	2 Observing Freq. and Bandwidth MHz	MHz	3 Field Centre RA(1950) H M S	DEC(1950) D M S	4 Observing Time Hours	5 Observing Date Year	Day	6 Interferometer Configuration	7 Halfpower Beam(arcs) RAxDEC	8 RMS Noise mJy/beam	9 Confusion Level in Total Intensity Map (mJy/beam)
3C 31	4995	10	01 04 39	32 08 44	1 x 12	79	104	54 LD	6 x 12	0.35	∿ 0.6
3C 33.1	4990	10	01 06 00	72 55 45	1 x 12	78	141	36 HD	7 x 7	0.35	∿ 0.6
	1412.6	10	01 05 01	72 56 05	1 x 12	77	360	36 HD	24 x 25	0.35	∿ 2.5
	608.5	2.5	01 06 06	72 56 05	1 x 12	78	316	36 HD	56 x 59	2.3	∿ 5
3C 35	4995	10	01 09 09	49 16 45	1 x 12	80	039	36 OLD	7 x 9	0.35	∿ 0.35
	4995	10	01 08 59	49 09 23	1 x 12	79	153	36 HD	7 x 9	0.25	∿ 0.25
	1412	10	01 09 03	49 12 00	1 x 12	78	008	72 OLD	24 x 32	0.5	∿ 0.50
	608.5	2.5	01 09 60	49 10 00	1 x 12	78	318	36 HD	56 x 74	1.4	∿ 10
3C 66 B	4995	10	02 20 04	42 45 30	1 x 12	79	112	54 HD	7 x 10	0.3	$\lesssim$ 4
	1415	4	02 19 30	42 46 01	1 x 12	75	173	36 OLD	24 x 36	0.3	∿ 5
	1415	4	"	"	1 x 12	75	187	72 OLD			
	609.8	4	02 20 00	42 48 00	1 x 12	73	253	72 OLD	56 x 83	1.5	$\lesssim$ 10
3C 129	4995	10	04 45 28	44 56 32	1 x 12	79	147	36 HD	7 x 10	0.25	$\lesssim$ 0.5 (head)
	4995	10	"	"	1 x 12	79	111	54 HD			
	609.5	4	04 44 46	44 55 00	1 x 12	77	041	36 OLD	56 x 79	0.75	∿ 12 (head)
	609.5	4	"	"		77	053	36 OLD			
	609.5	4	"	"	1 x 12	77	064	54 OLD			
	609.5	4	"	"	1 x 12	77	078	72 OLD			
	609.5	4	"	"	1 x 12	77	071	90 OLD			
3C 130	4874	10	04 48 57	51 59 45	1 x 12	78	121	36 HD	7 x 9	0.5	∿ 1.5
	1412.6	10	04 49 00	52 00 00	1 x 12	78	013	36 HD	24 x 31	0.35	∿ 1
	608.5	2.5	04 48 57	51 59 56		78	311	36 HD			
	608.5	2.5	"	"	1 x 12	78	312	36 HD	56 x 72	1.3	∿ 5
	608.5	2.5	"	"		78	338	36 HD			
3C 223	4995	10	09 36 51	36 07 35	1 x 12	79	106	54 LD	6 x 10	0.4	∿ 1
	1415	4	09 36 51	36 07 35	1 x 12	77	175	54 LD	22 x 37	0.5	∿ 4
	1415	4	"	"		77	184	54 LD			
3C 310	4995	10	15 02 47	26 12 36	1 x 12	79	100	54 LD	6 x 14	0.3	∿ 1
	608.5	2.5	15 02 48	26 12 30	1 x 12	78	296	54 LD	51 x 115	1.2	∿ 12
3C 390.3	4995	10	18 45 34	79 43 30	1 x 12	79	140	36 OLD	7 x 7	0.40	∿ 20
	608.5	2.5	18 45 38	79 43 06	1 x 12	78	340	36 HD	24 x 24	2.0	∿ 100
4C 48.29	4874	10	10 17 45	48 45 52	1 x 12	78	120	36 HD	7 x 9	0.3	∿ 1
	4874	10	"	"	1 x 12	78	155	54 HD			
	1415	4	10 18 00	48 45 00	1 x 12	77	192	36 OLD	25 x 33	0.4	∿ 1
	608.5	2.5	10 18 00	48 45 00	1 x 12	78	313	36 HD	56 x 75	1.5	∿ 7

+ Interferometer configuration (see also Table 3):
OLD = Old configuration (20 interferometers, 72 m increments)
HD = High Density Array (40 interferometers, 36 m increments)
LD = Low Density Array (40 interferometers, 36 m increments except at shortest baselines to minimize shadowing of the telescope)

TABLE III.

Interferometer Configuration	Interferometer Spacings (m) shortest/increment/longest		
36 OLD	36	72	1404
54 OLD	54	72	1422
72 OLD	72	72	1440
90 OLD	90	72	1458
36 HD	36	36	1440
54 HD	54	36	1458
54 LD	54	36,72	1602

TABLE IV.

Source	Wavelength [cm]	Total flux density [Jy]	Percentage Polarization	Polarization Position Angle [degrees]
3C 31	6	1.66 ± 0.13	2.7 ± 0.6	35 ± 7
3C 33.1	6	0.98 ± 0.10	12.4 ± 2.0	123 ± 5
	21	3.26 ± 0.26	3.2 ± 0.7	91 ± 7
	49[1)]	4.94 ± 0.40	0.7 ± 0.5	100 ± 20
3C 35, S. Lobe	6	0.29 ± 0.05	2.8 ± 0.7	33 ± 7
N. Lobe	6[2)]	0.46 ± 0.07	$\lesssim$ 0.5	---
	21	2.28 ± 0.18	4.0 ± 0.8	78 ± 6
	49[1)]	3.52 ± 0.28	3.0 ± 0.7	144 ± 7
3C 66B	6	2.83 ± 0.23	6.9 ± 1.2	76 ± 5
	21	8.86 ± 0.71	1.5 ± 0.6	77 ± 11
	49	16.7 ± 1.3	---	---
3C 129	6	2.36 ± 0.19	5.0 ± 0.9	15 ± 5
	49	15.6 ± 1.3	---	---
3C 130	6	0.98 ± 0.08	5.5 ± 1.0	134 ± 5
	21	3.02 ± 0.24	2.1 ± 0.6	130 ± 8
	49[1)]	4.74 ± 0.38	---	---
3C 223	6	1.31 ± 0.10	8.2 ± 1.3	82 ± 5
	21	3.57 ± 0.29	8.2 ± 1.3	118 ± 5
3C 310	6	1.25 ± 0.10	1.8 ± 0.6[3)]	17 ± 10[3)]
	49	19.3 ± 1.5	1.9 ± 0.6	164 ± 9
3C 390.3	49	20.3 ± 1.6	2.9 ± 0.7	18 ± 7
4C 48.29	6	0.67 ± 0.05	5.4 ± 1.0	120 ± 5
	21	1.69 ± 0.14	3.5 ± 0.7	119 ± 6
	49	3.64 ± 0.29	3.8 ± 0.8	51 ± 6

Notes:

1. Flux missing because of missing short spacings due to interference or other problems.
2. Core included.
3. Using full resolution (i.e. unconvolved) map, large scale low brightness polarization below detection level.

TABLE V.

Source	Radio Core Positions RA(1950) H M S	DEC(1950) D M S	Flux density at 6 cm (mJy)	Magnitude V	Redshift Z	Luminosity+ Distance (Mpc)	Angular Size++ Conversion Ratio (kpc/arcsec)	References Z
3C 31	(core confused with jet)		-	12.1	.0169	51	0.24	1
3C 33.1	01 06 06.34±0.12	72 55 58.6±0.3	15±1	19.5-20	.173	539	1.90	2
3C 35	01 09 04.93±0.07	49 12 40.6±0.7	14±3	15	.0677	206	0.88	3
3C 66^{B}	(core confused with jet)		-	12.9	.0215	65	0.30	4
3C 129	04 45 31.92±0.05	44 55 29.0±0.3	34±4	19.4	.0208	63	0.29	5
3C 130	04 48 57.29±0.06	51 59 50.2±0.3	28±1	16.5	.1090	335	1.32	6
3C 223	09 36 50.81±0.05	36 07 38.3±0.5	8.5±1.0	17.1	.1371	424	1.59	7
3C 310	15 02 46.90±0.04	26 12 35.3±0.5	89.0±1.6	15.2	.0540	164	0.72	8
3C 390.3	18 45 37.44±0.19	79 43 06.8±0.2	340±8	14.5	.0569	173	0.75	9
4C 48.29	10 17 47.65±0.05	48 46 32.7±0.3	74.5±2.6	16	.052	158	0.69	8

+ Assuming a Hubble constant H_o = 100 km sec^{-1}mpc^{-1} and q_o = 0.5.

++ Using the Angular Size Distance.

References for Z

1. Humason et al., 1956
2. Sargent, 1977; Longair and Gunn, 1975
3. Burbidge and Strittmatter, 1972
4. Maltby et al., 1963
5. Spinrad, 1975
6. Smith et al., 1976
7. Sandage, 1978
8. Miley and Osterbrock, 1979
9. Osterbrock et al., 1975

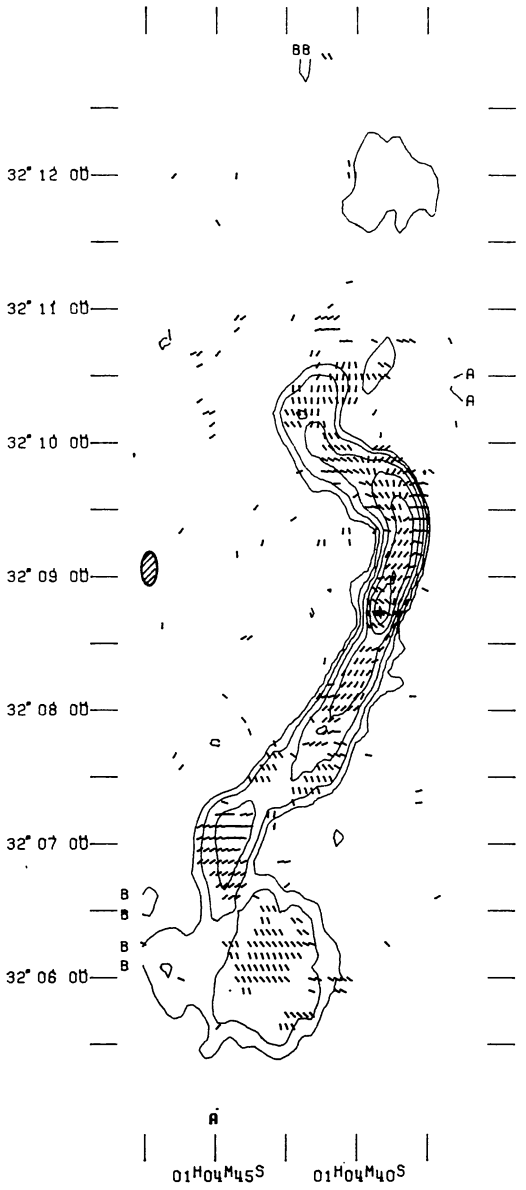

FIGURE 1. — 3C 31, 6 cm I + ϕ ; – 2.5, 2.5, 5, 10, 20, 40, 80 mJy/beam.

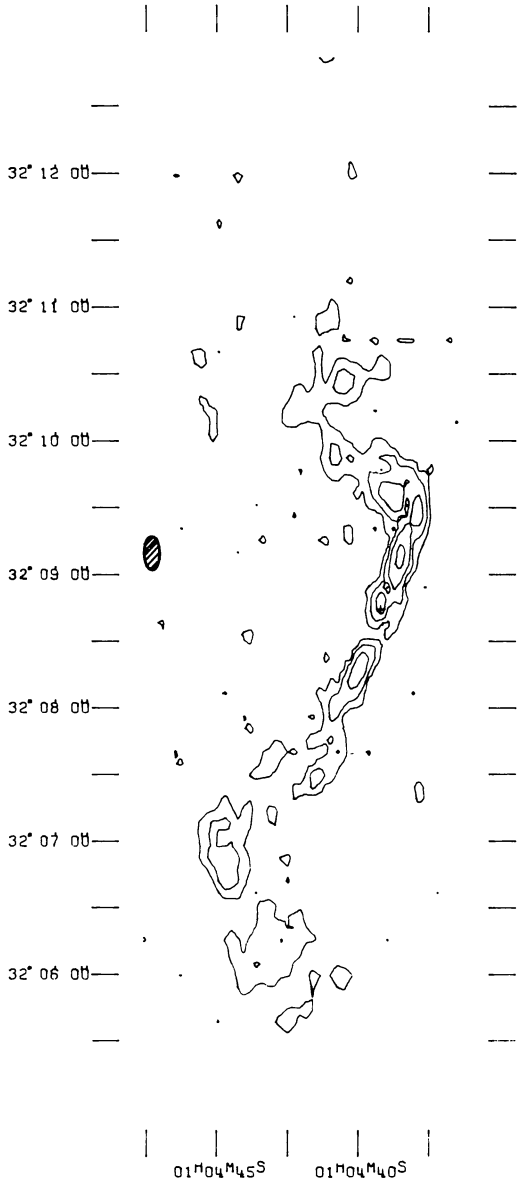

FIGURE 2. — 3C 31, 6 cm P ; 1, 2, 4, 8 mJy/beam.

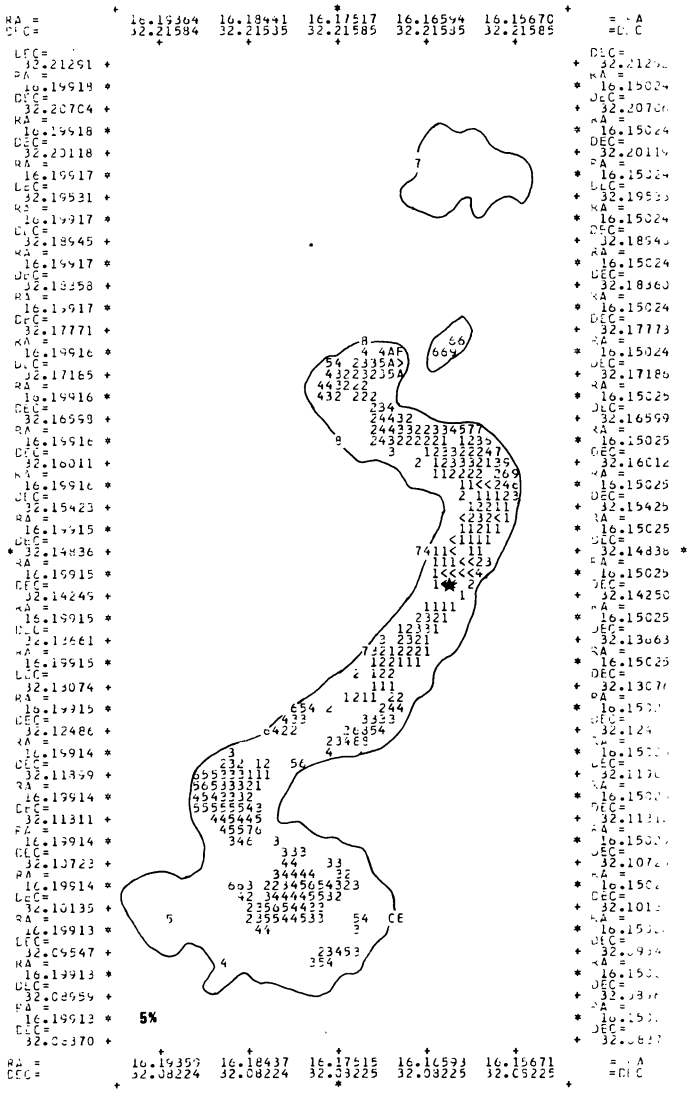

FIGURE 3. — 3C 31, 6 cm % ; 2.5 mJy/beam.

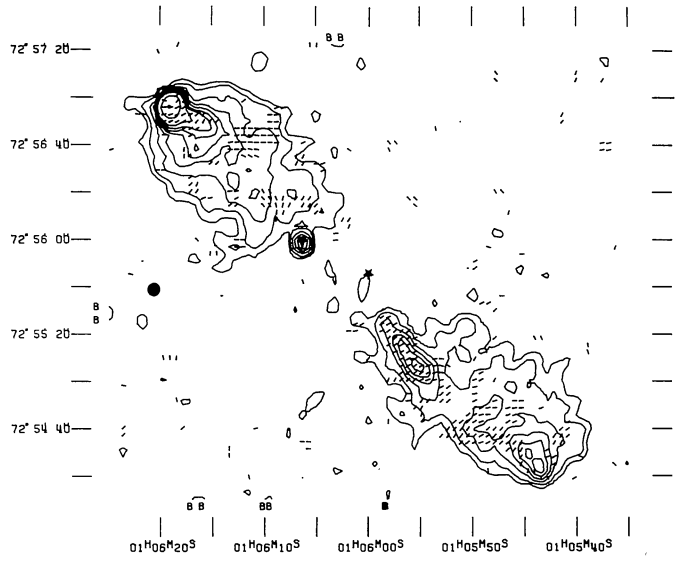

FIGURE 4. — 3C 33.1, 6 cm I + ϕ ; − 2.5, 1.25, 2.5, 5, 7.5, 10, 12.5, 15, 20, 40, 80 mJy/beam.

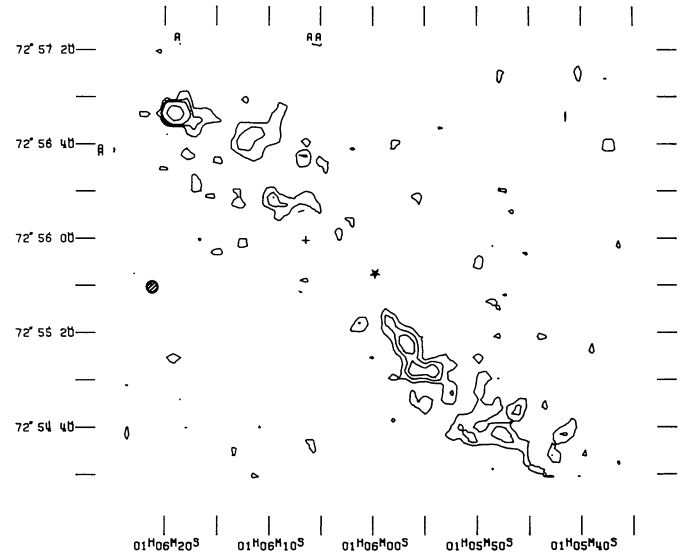

FIGURE 5. — 3C 33.1, 6 cm P ; 1.5, 2.25, 3, 6 mJy/beam.

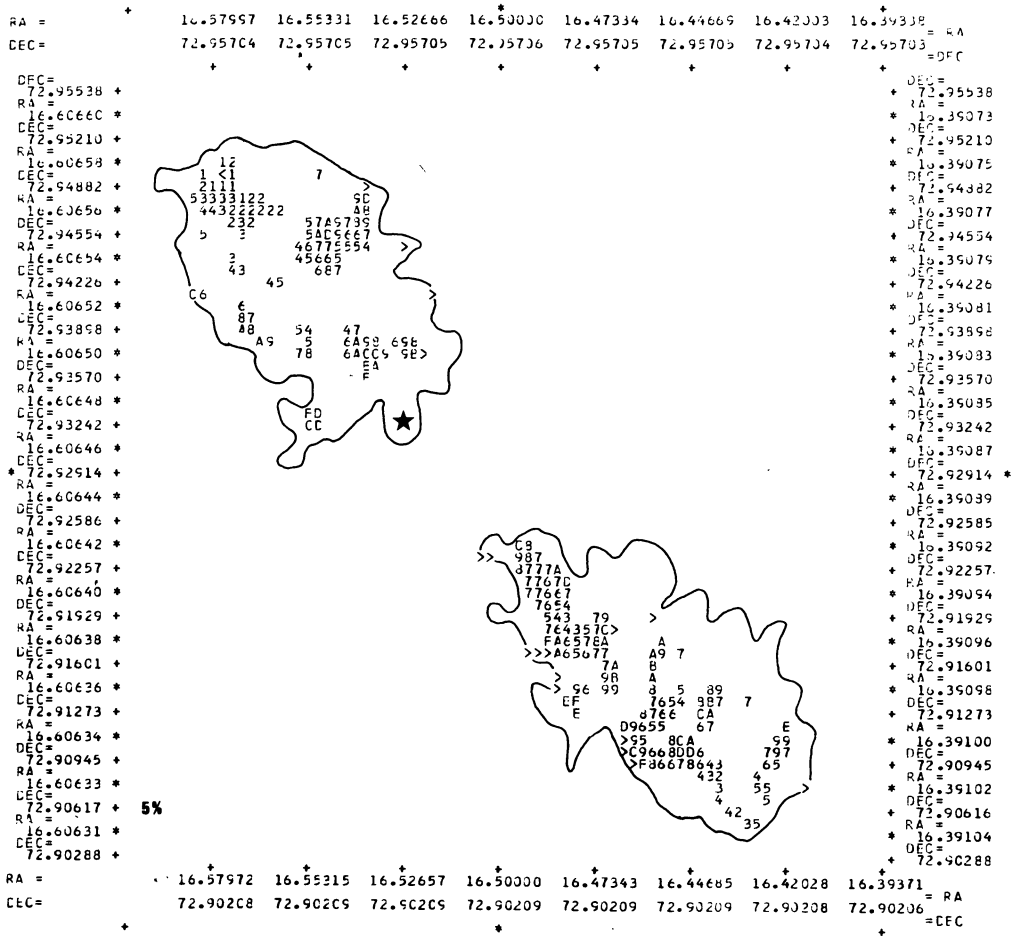

FIGURE 6. — 3C 33.1, 6 cm % ; 1.25 mJy/beam.

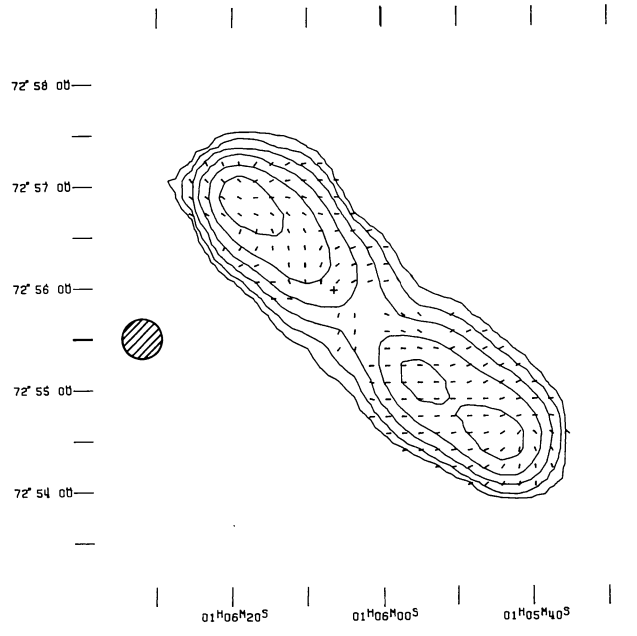

FIGURE 7. — 3C 33.1, 21 cm I + ϕ ;
– 10, 10, 20, 40, 80, 160, 320 mJy/beam.

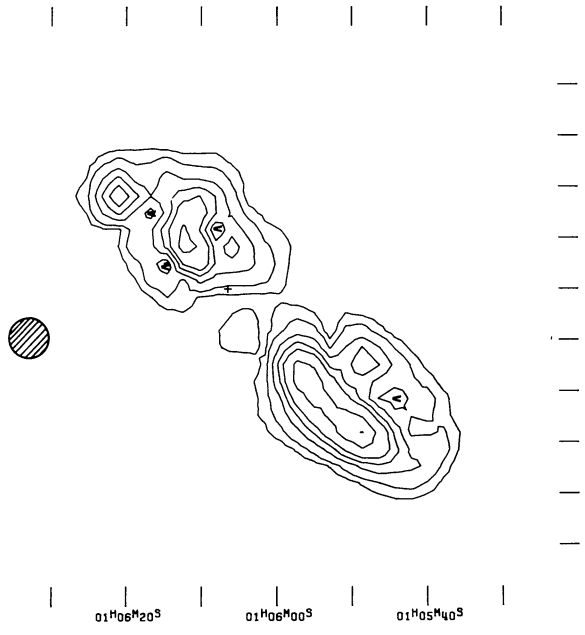

FIGURE 8. — 3C 33.1, 21 cm P ;
2, 4, 8, 12, 16, 24, 32 mJy/beam.

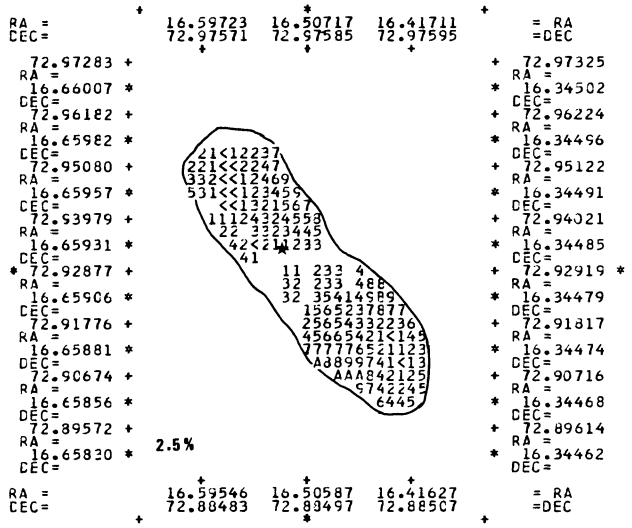

FIGURE 9. — 3C 33.1, 21 cm % ; 10 mJy/beam.

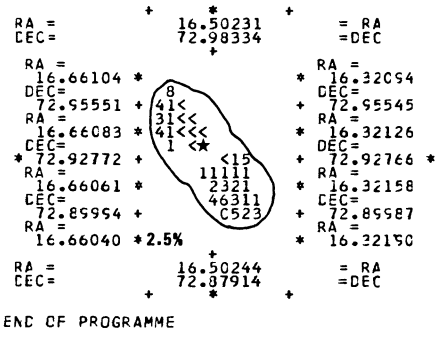

FIGURE 11. — 3C 33.1, 49 cm % ; 20 mJy/beam.

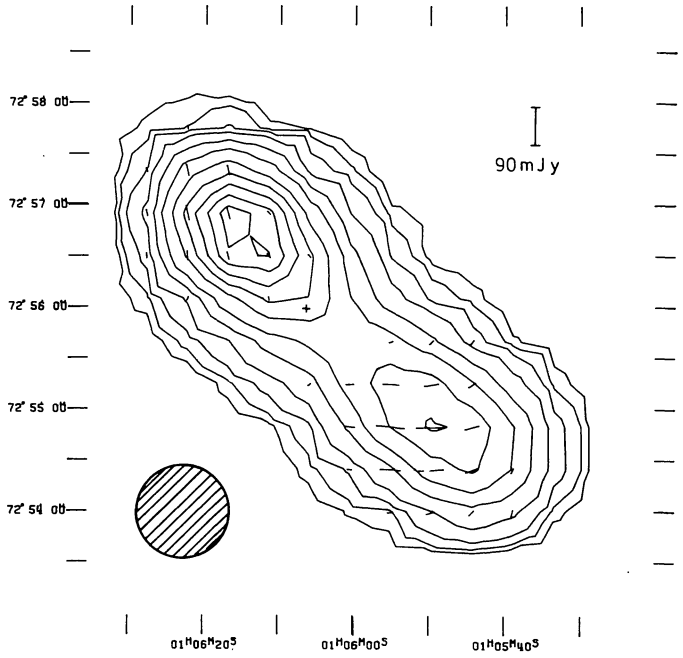

FIGURE 10. — 3C 33.1, 49 cm I + ϕ ; − 20, 20, 40, 80, 160, 320, 500, 750, 1000, 1250, 1500, 1750 mJy/beam.

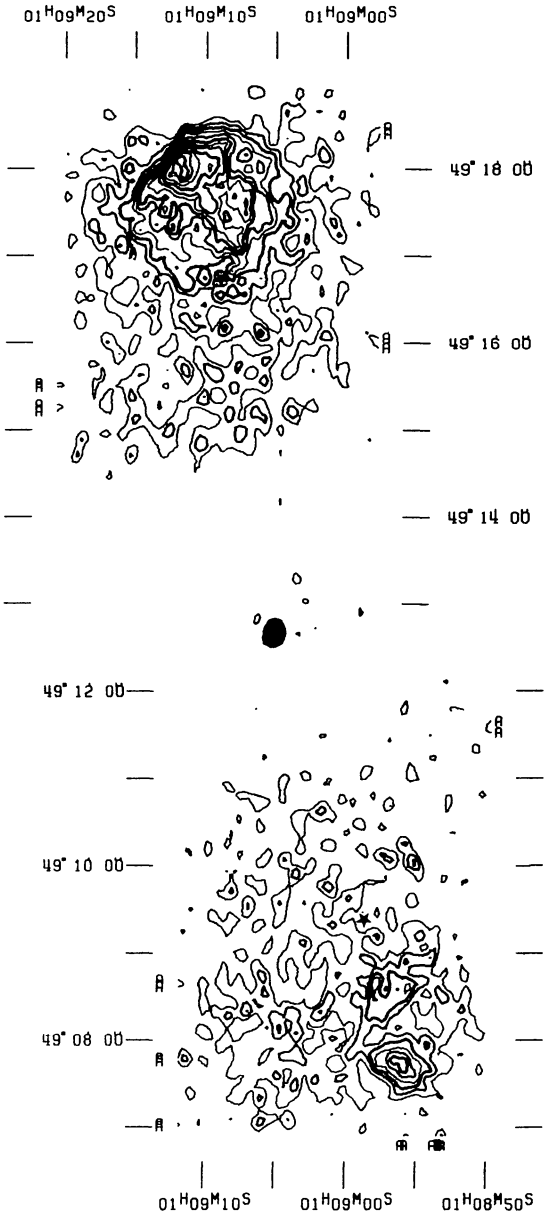

FIGURE 12. — 3C 35, 6 cm I ; .5, 1, 1.5, 2, 2.5, 3, 3.5, 4, 5, 6, 7, 8 mJy/beam.

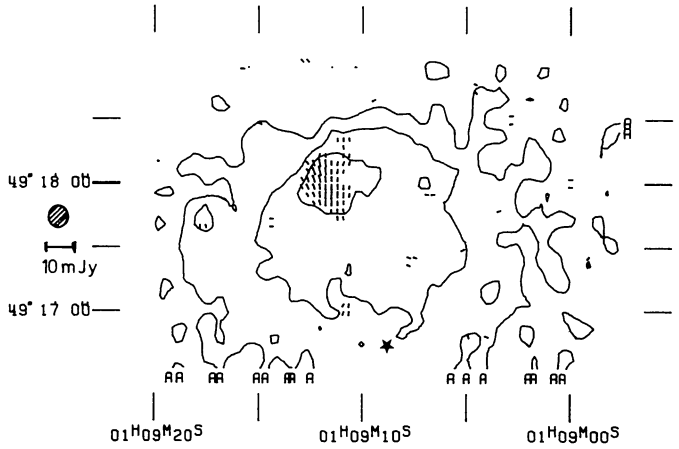

FIGURE 13. — 3C 35, 6 cm I + ϕ (N. Lobe) ; .5, 2, 5 mJy/beam.

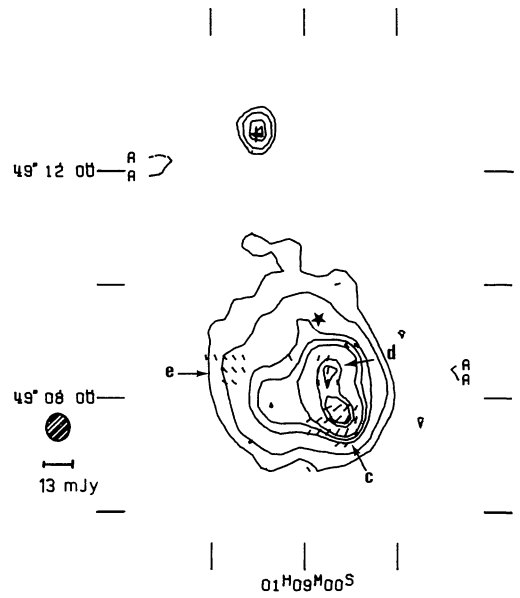

FIGURE 15. — 3C 35, 6 cm I + ϕ convolved (S. Lobe) ; − 2, 2, 4, 8, 10, 12, 18, 20 mJy/beam.

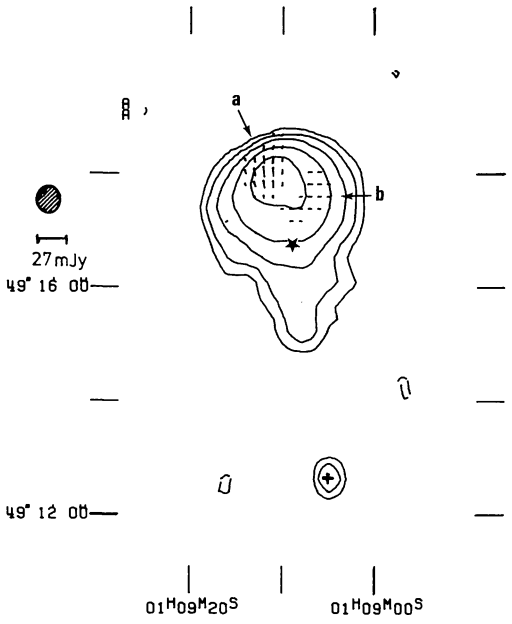

FIGURE 14. — 3C 35, 6 cm I + ϕ convolved (N. Lobe) ; − 1, 2, 4, 8, 16, 32 mJy/beam.

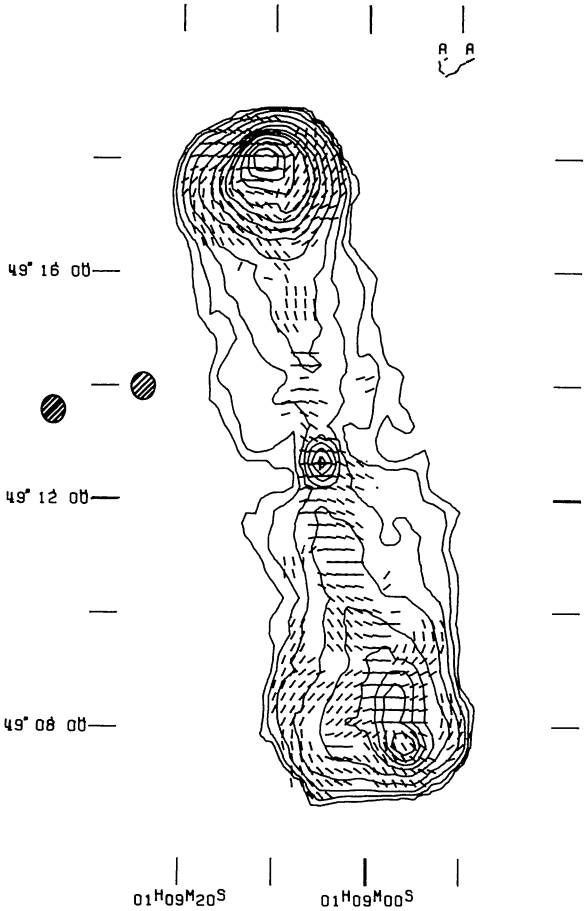

FIGURE 16. — 3C 35, 21 cm I + ϕ ; − 2, 1, 2, 4, 8, 15, 22.5, 30, 37.5, 45, 60, 75, 90 mJy/beam.

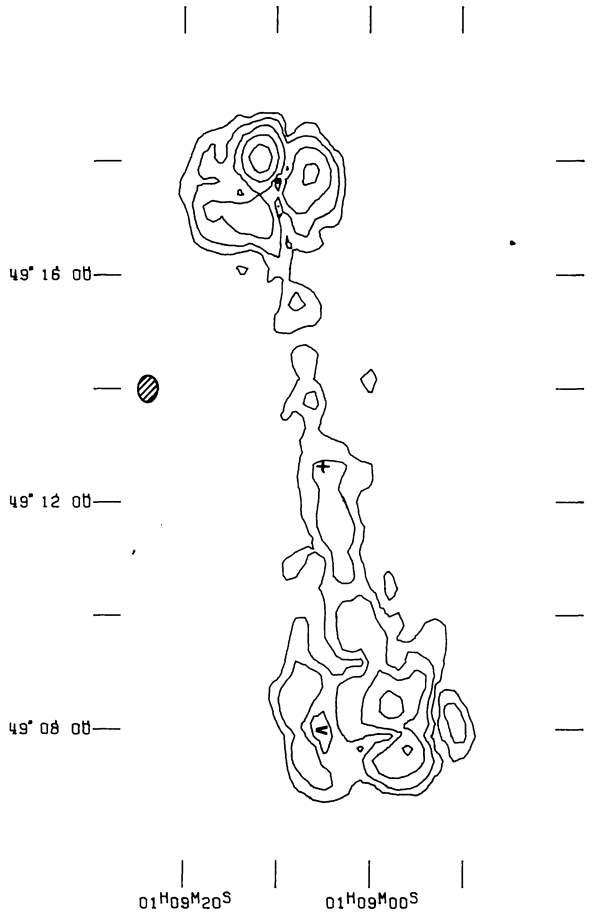

FIGURE 17. — 3C 35, 21 cm P ; 1, 2, 4, 8, 16 mJy/beam.

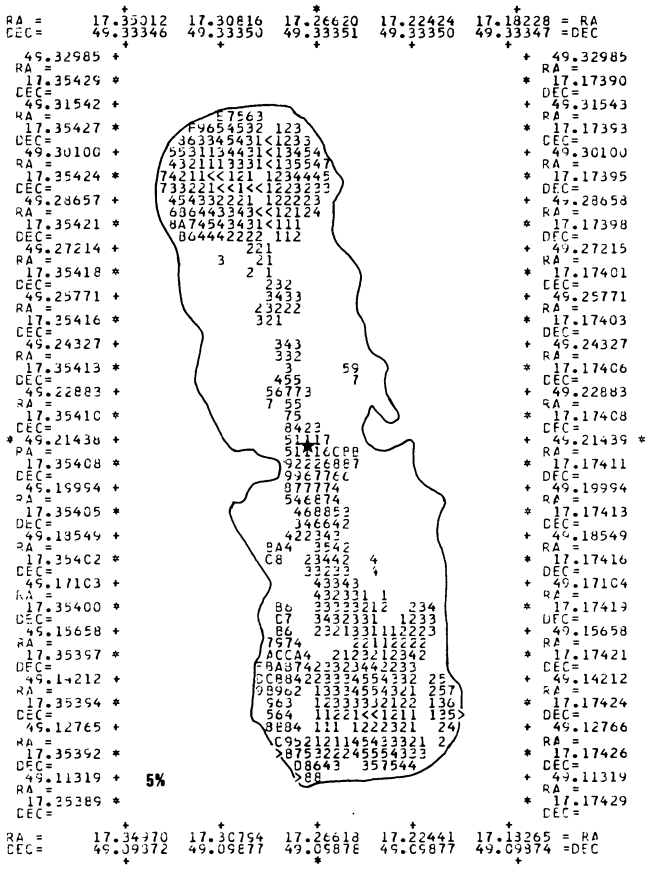

FIGURE 18. — 3C 35, 21 cm % ; 1 mJy/beam.

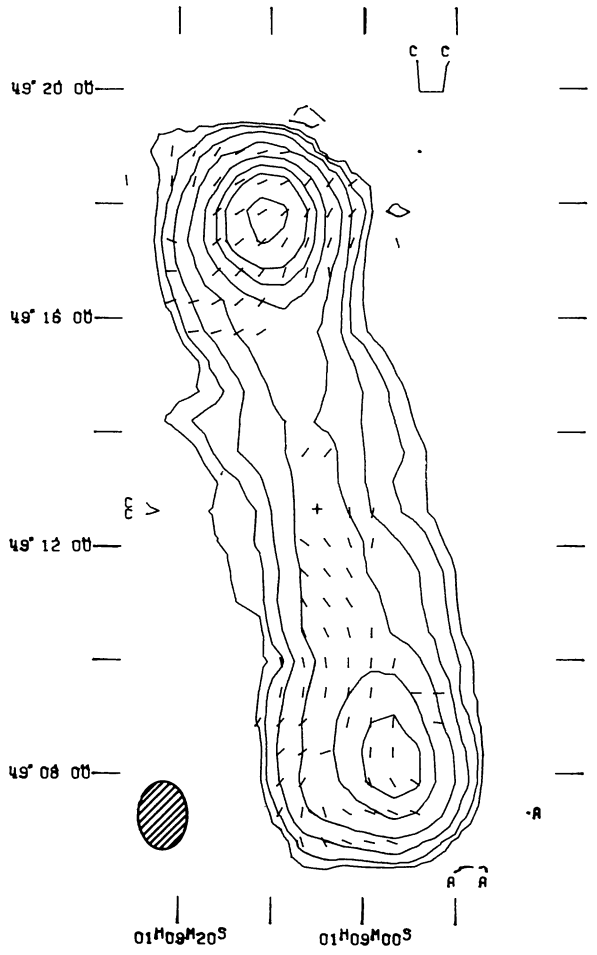

FIGURE 19. — 3C 35, 49 cm I + ϕ ;
– 10, 10, 20, 40, 80, 160, 240, 320, 500 mJy/beam.

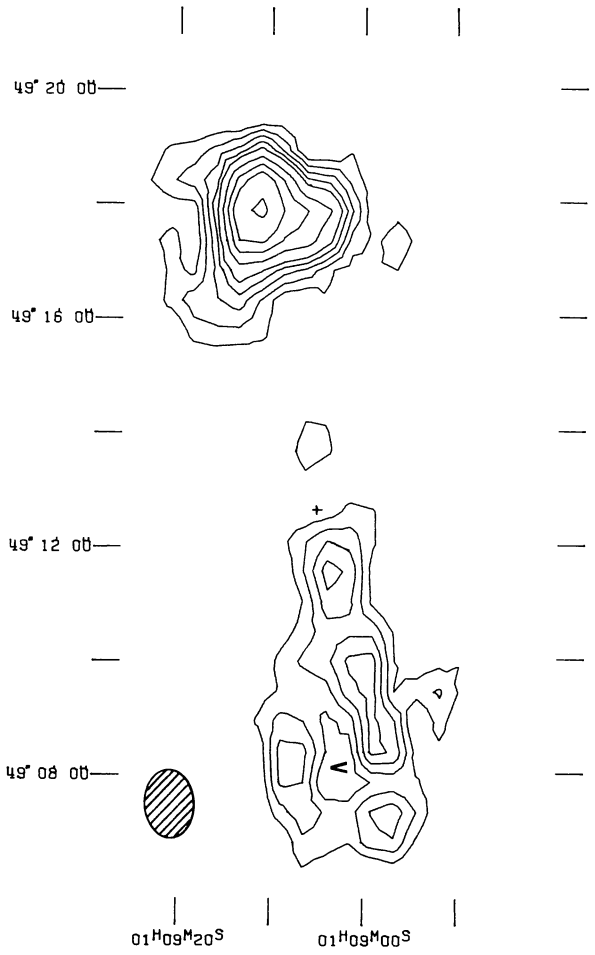

FIGURE 20. — 3C 35, 49 cm P ;
6, 9, 12, 15, 18, 24, 30, 36, 48 mJy/beam.

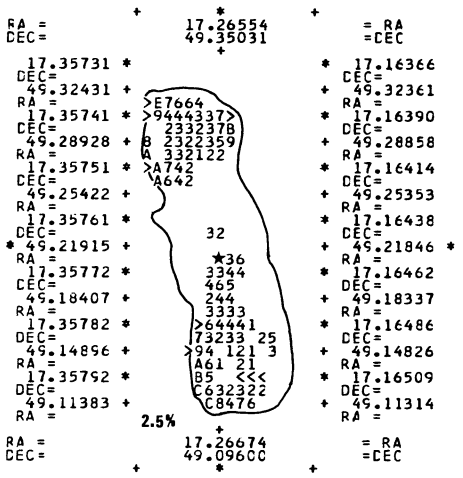

FIGURE 21. — 3C 35, 49 cm % ; 10 mJy/beam.

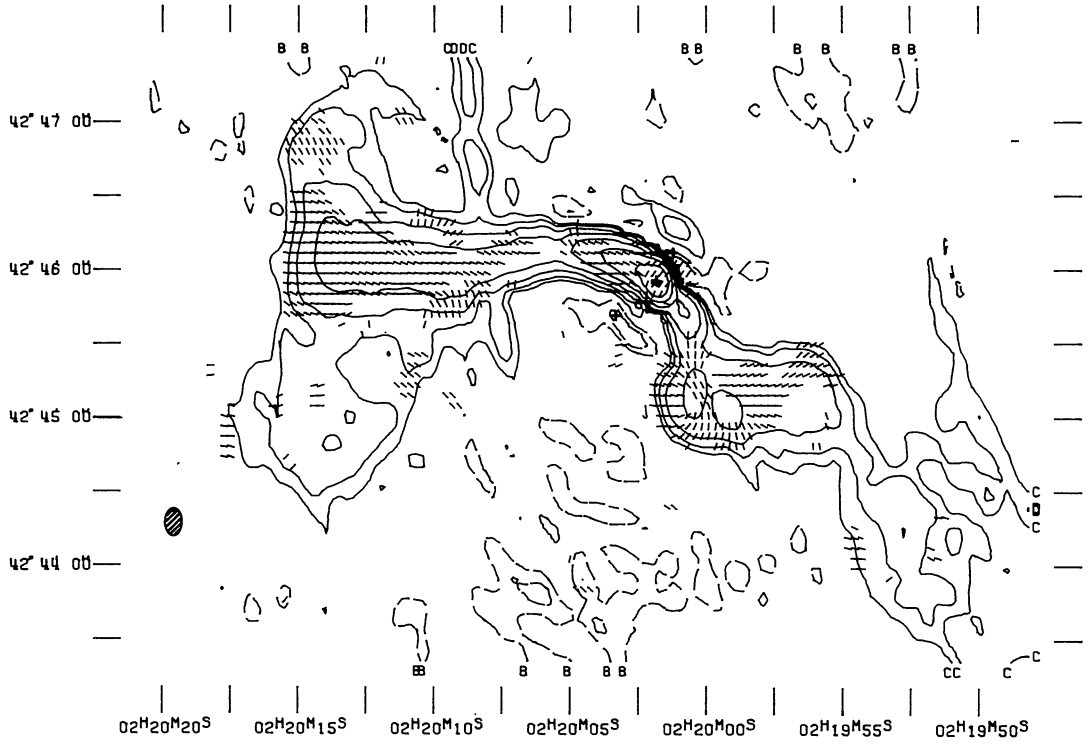

FIGURE 22. — 3C 66B, 6 cm I + ϕ ; − 4, − 2, 2, 4, 8, 16, 32, 64, 125, 250 mJy/beam.

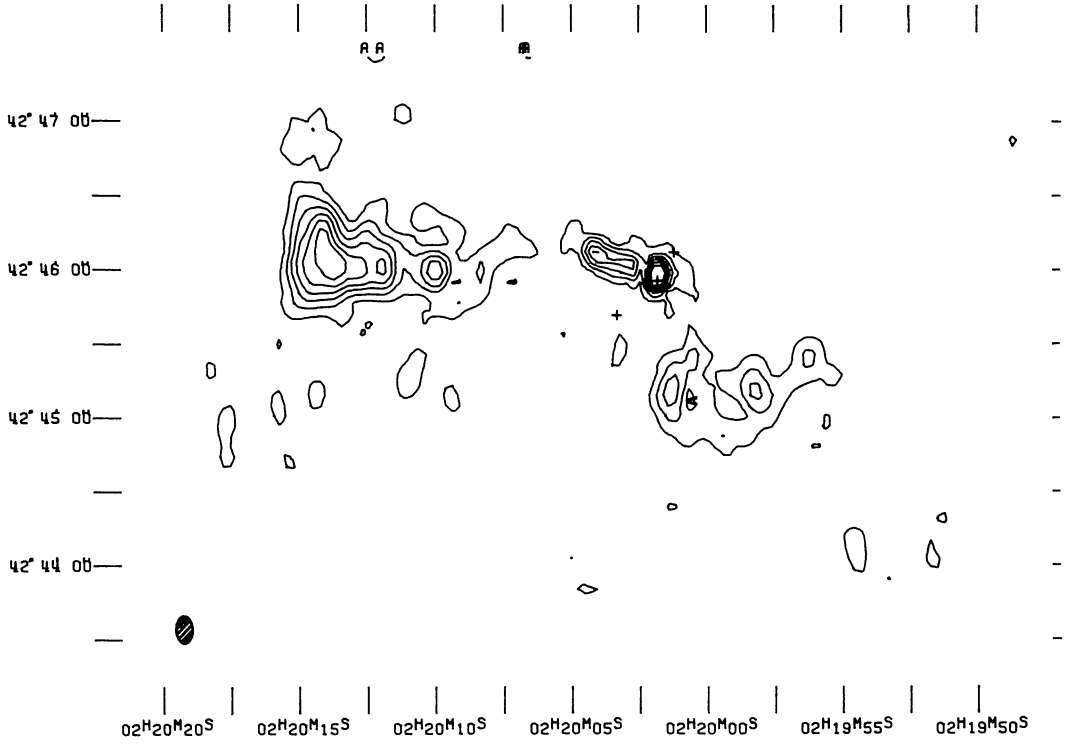

FIGURE 23. — 3C 66B, 6 cm P ; 1.5, 3, 4.5, 6, 7.5, 9 mJy/beam.

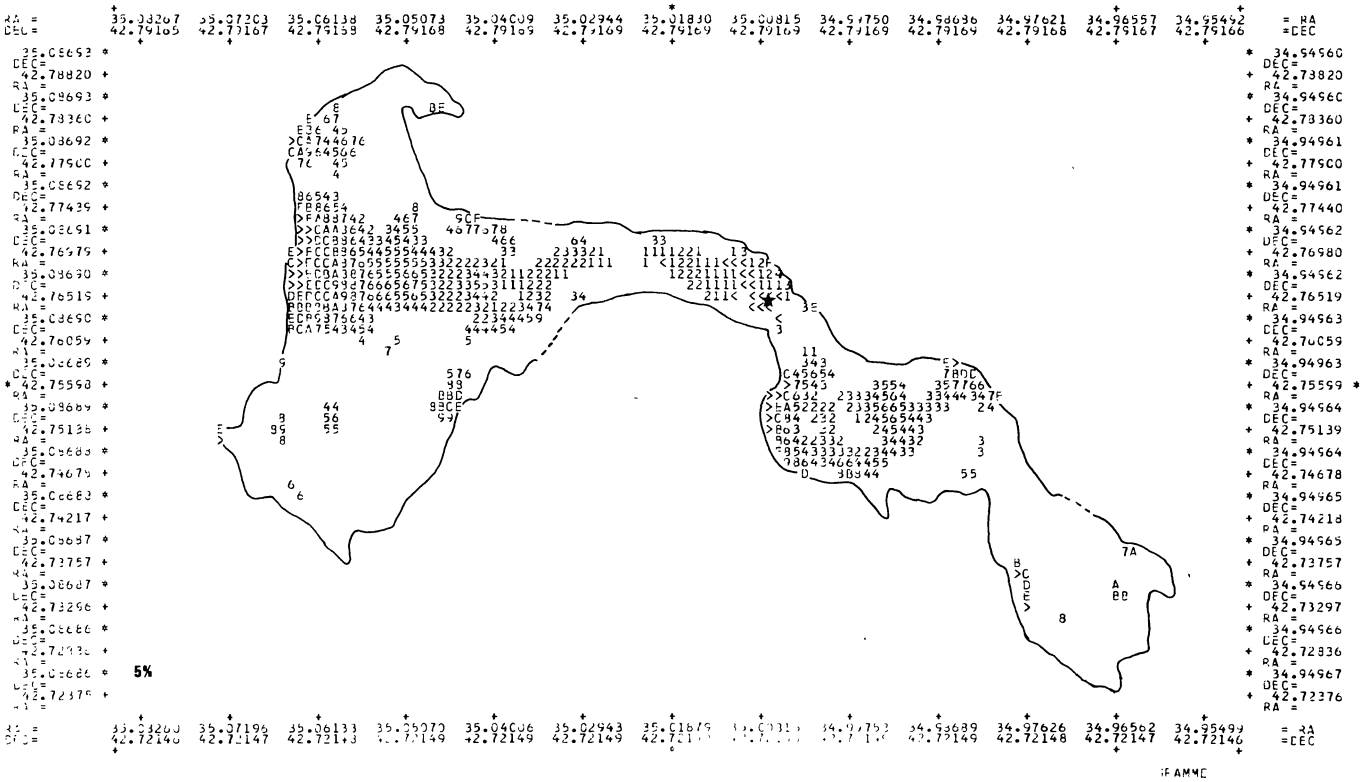

FIGURE 24. — 3C 66B, 6 cm % ; 2 mJy/beam.

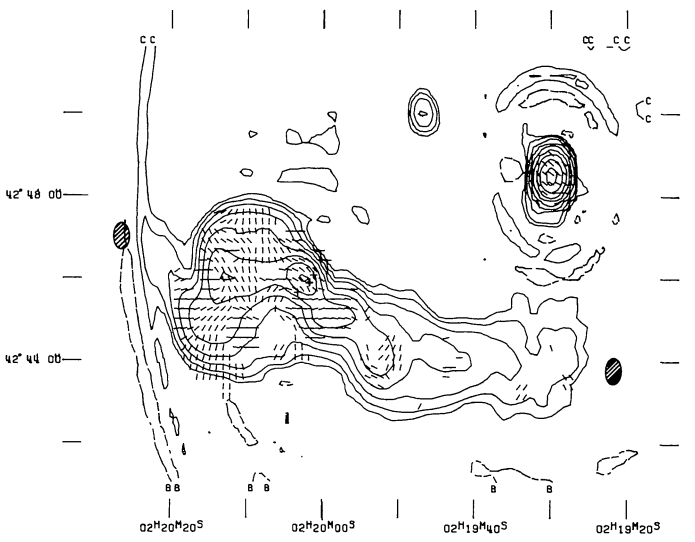

FIGURE 25 (top). — 3C 66B, 21 cm I + ϕ ; – 5, 5, 10, 20, 40, 80, 160, 320, 640, 1280 mJy/beam.

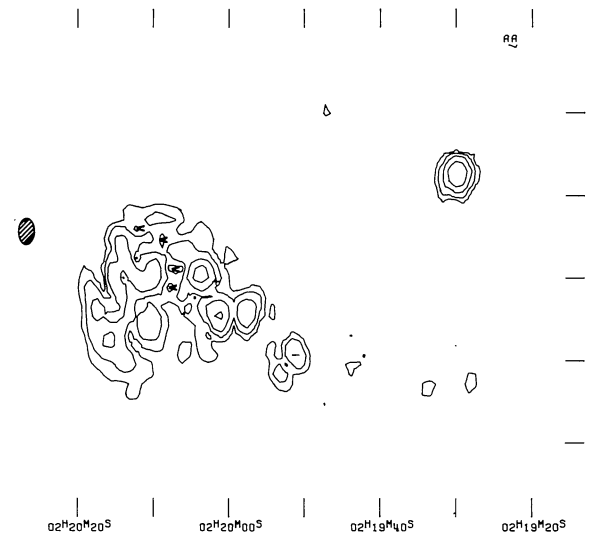

FIGURE 26 (bottom). — 3C 66B, 21 cm P ; 2.5, 5, 10, 20 mJy/beam.

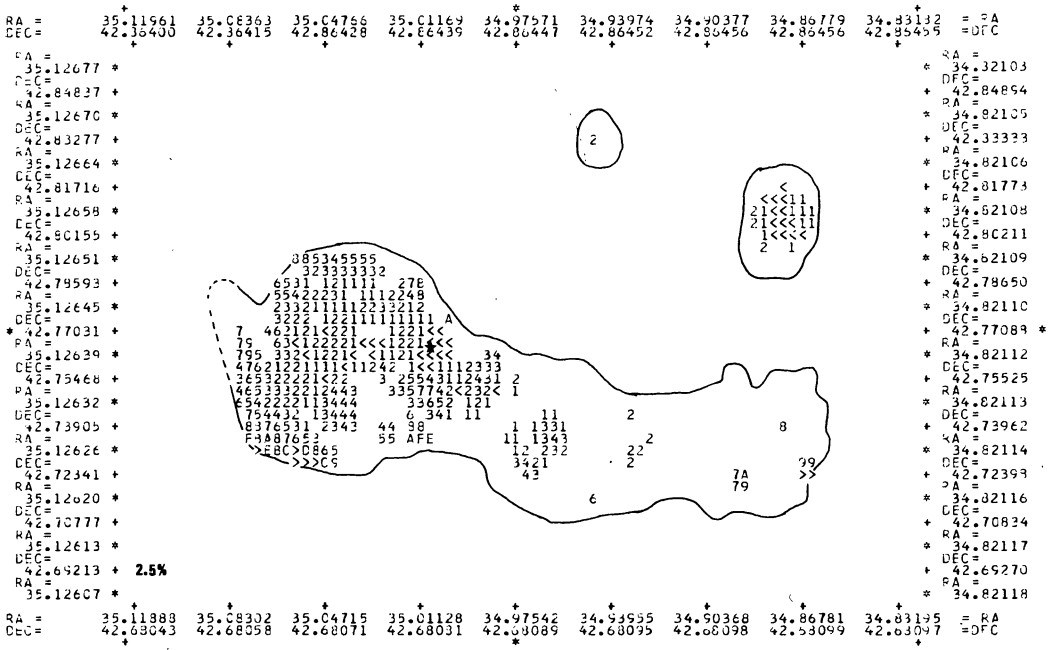

FIGURE 27. — 3C 66B, 21 cm % ; 5 mJy/beam.

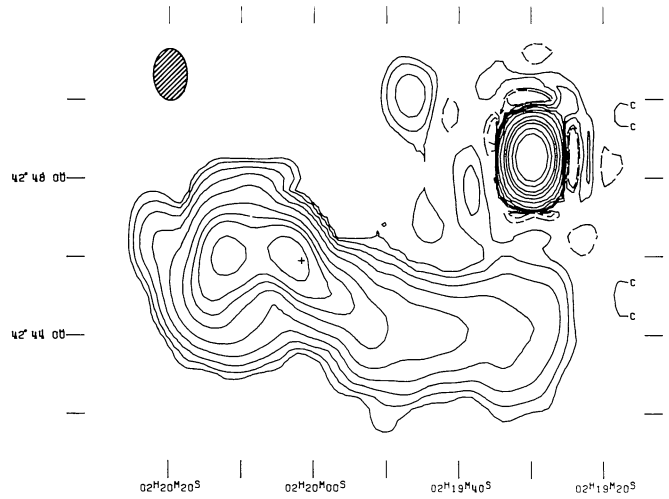

FIGURE 28. — 3C 66B, 49 cm I ; – 30, – 15, 15, 30, 60, 120, 240, 480, 720, 960, 1440, 1920 mJy/beam.

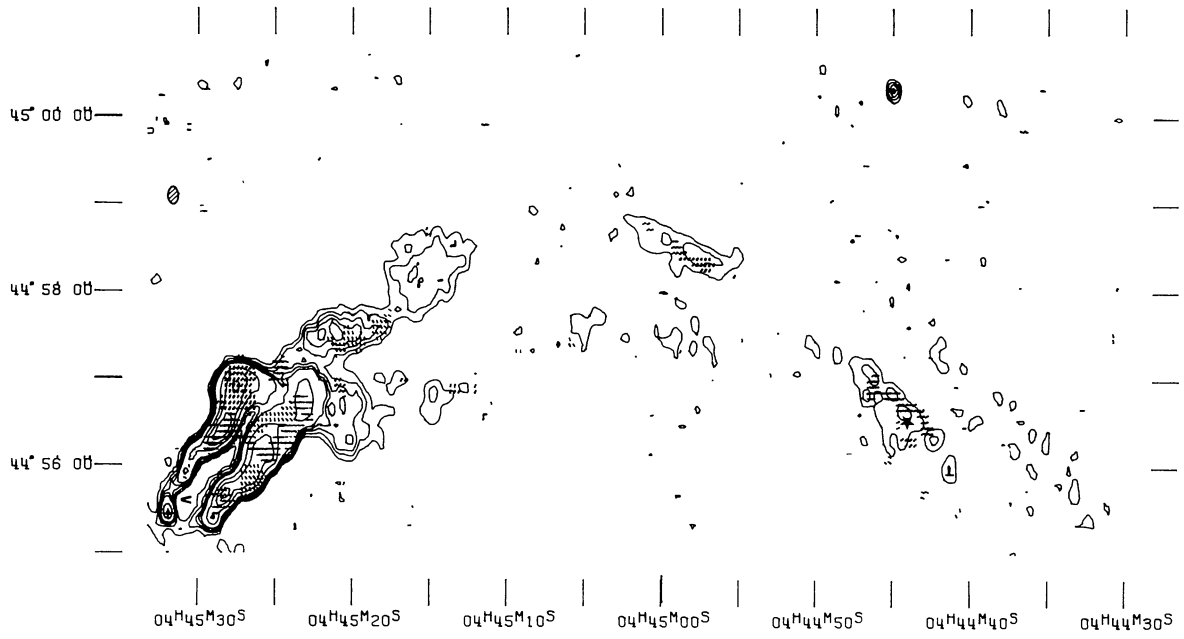

FIGURE 29. — 3C 129, 6 cm I + ϕ ; – 1, .5, 1, 1.5, 2, 2.5, 6, 7.5, 10 mJy/beam.

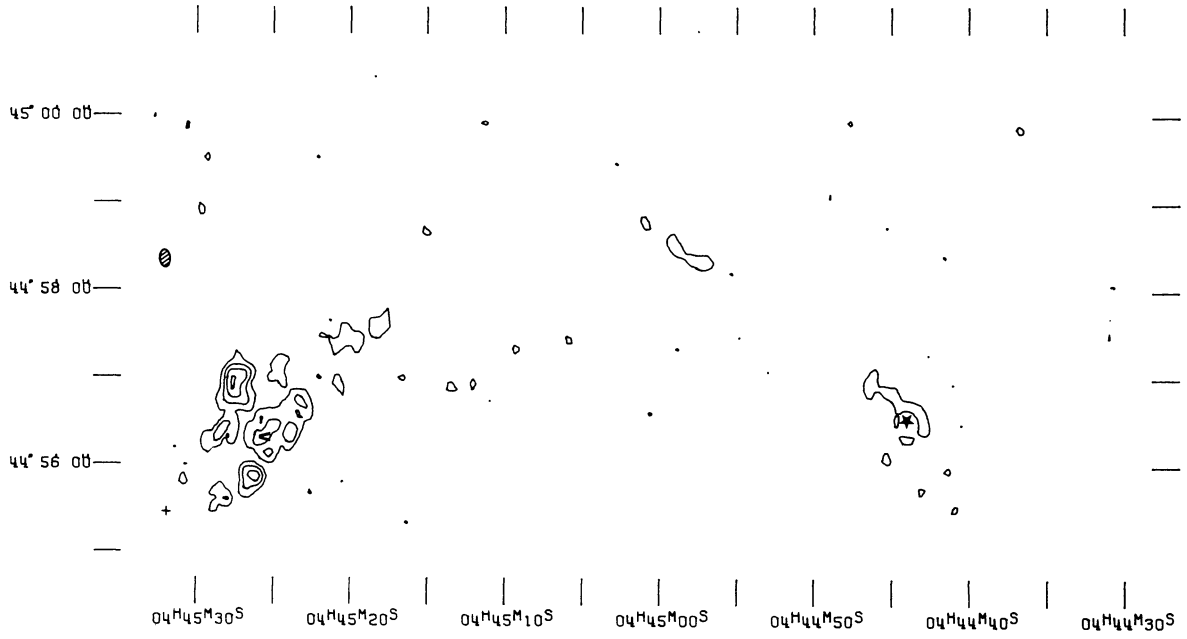

FIGURE 30. — 3C 129, 6 cm P ; .75, 1.5, 2.25, 3 mJy/beam.

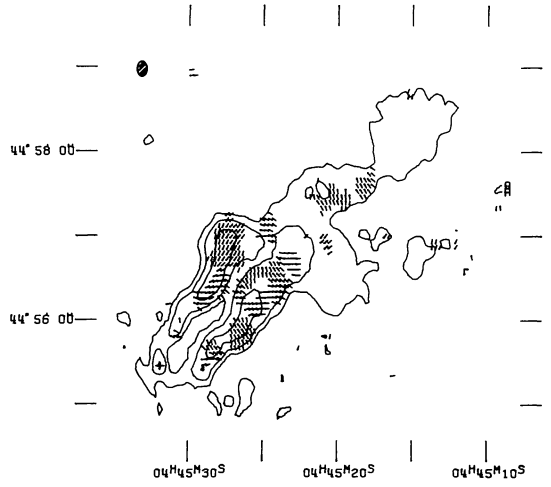

FIGURE 31. — 3C 129 (head), 6 cm I + ϕ ; .5, 2.5, 7.5 mJy/beam.

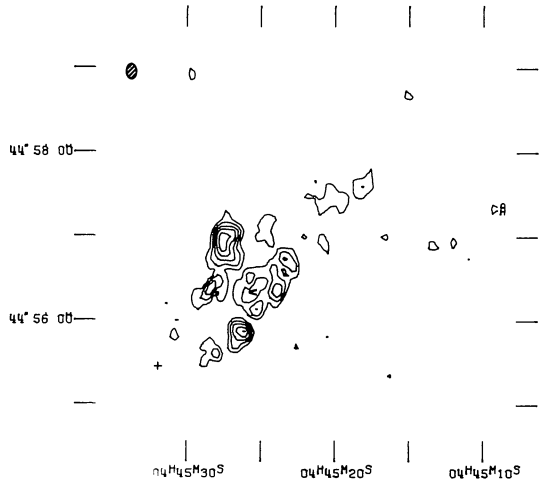

FIGURE 32. — 3C 129, 6 cm P ; .75, 1.25, 1.75, 2.25, 2.75 mJy/beam.

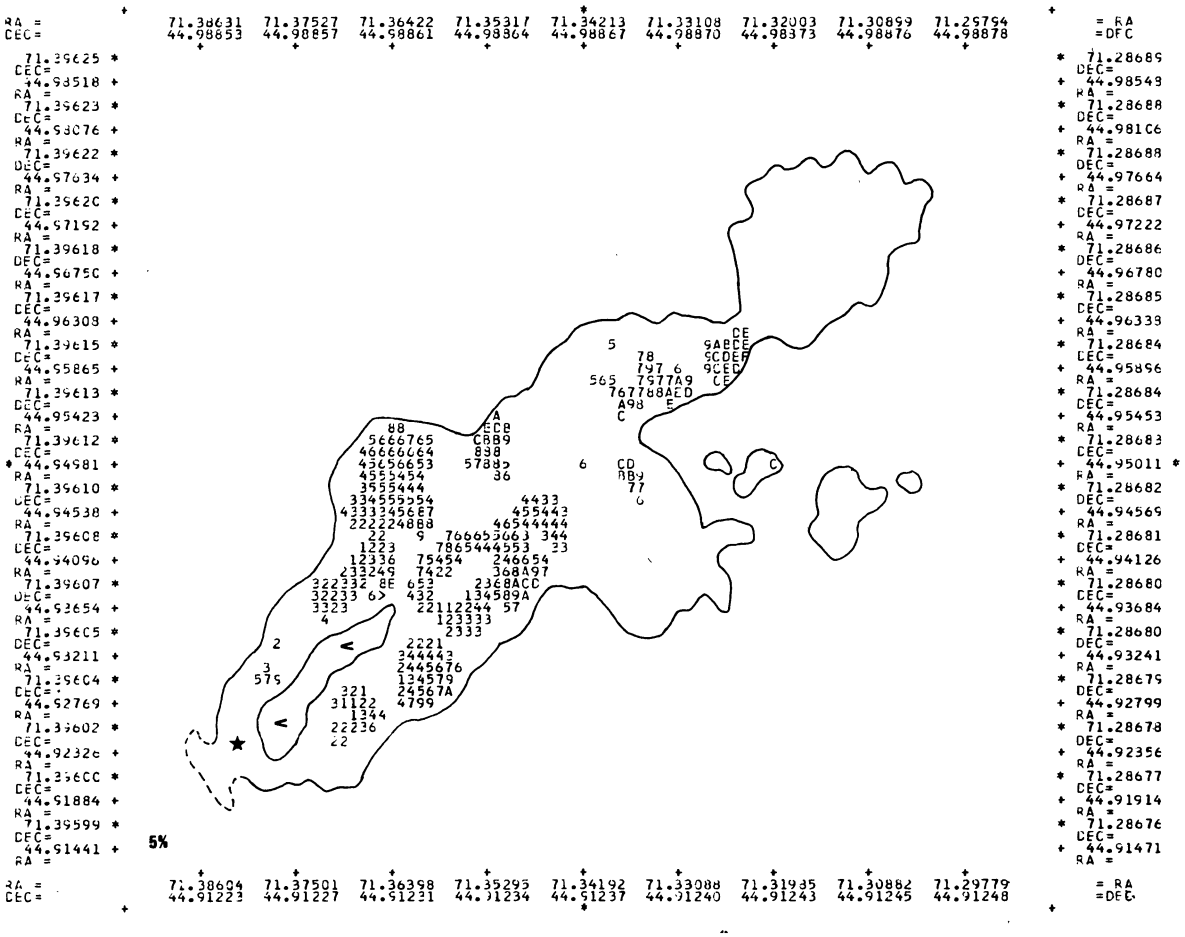

FIGURE 33. — 3C 129, 6 cm % ; .5 mJy/beam.

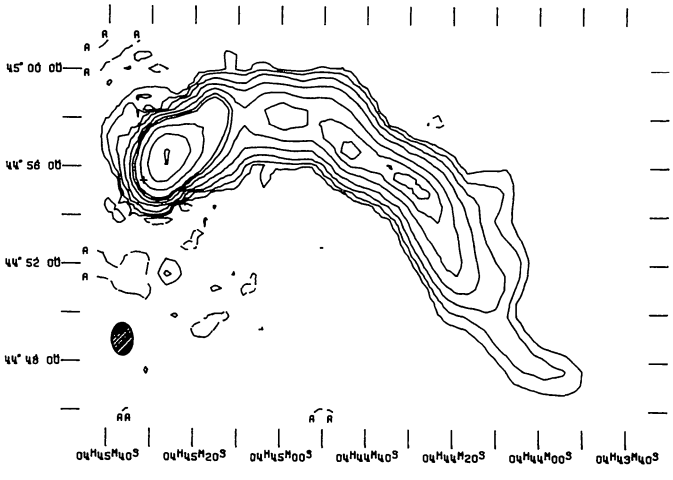

FIGURE 34. — 3C 129, 49 cm I ;
– 5, 10, 20, 40, 80, 160, 250, 320, 640, 1280, 2560 mJy/beam.

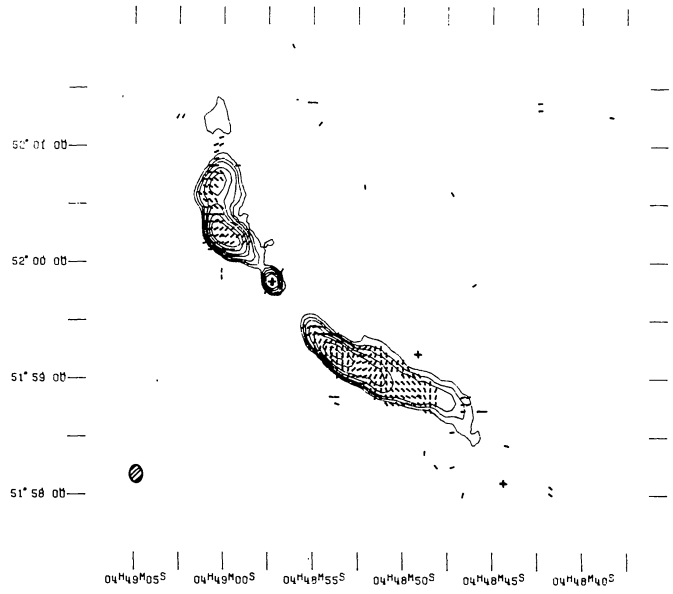

FIGURE 35. — 3C 130, 6 cm I + ϕ ;
– 4, 4, 6, 8, 12, 16, 24, 32, 48 mJy/beam.

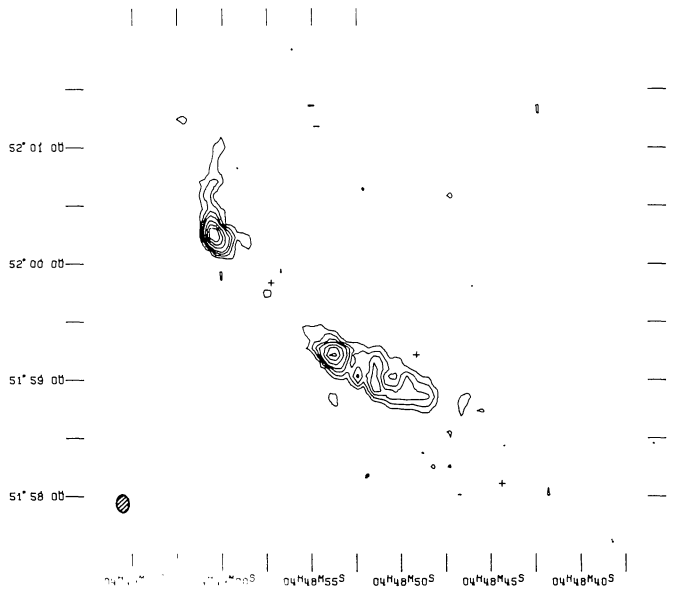

FIGURE 36. — 3C 130, 6 cm P ;
1.5, 2.5, 3.5, 4.5, 6.5, 8.5, 10.5 mJy/beam.

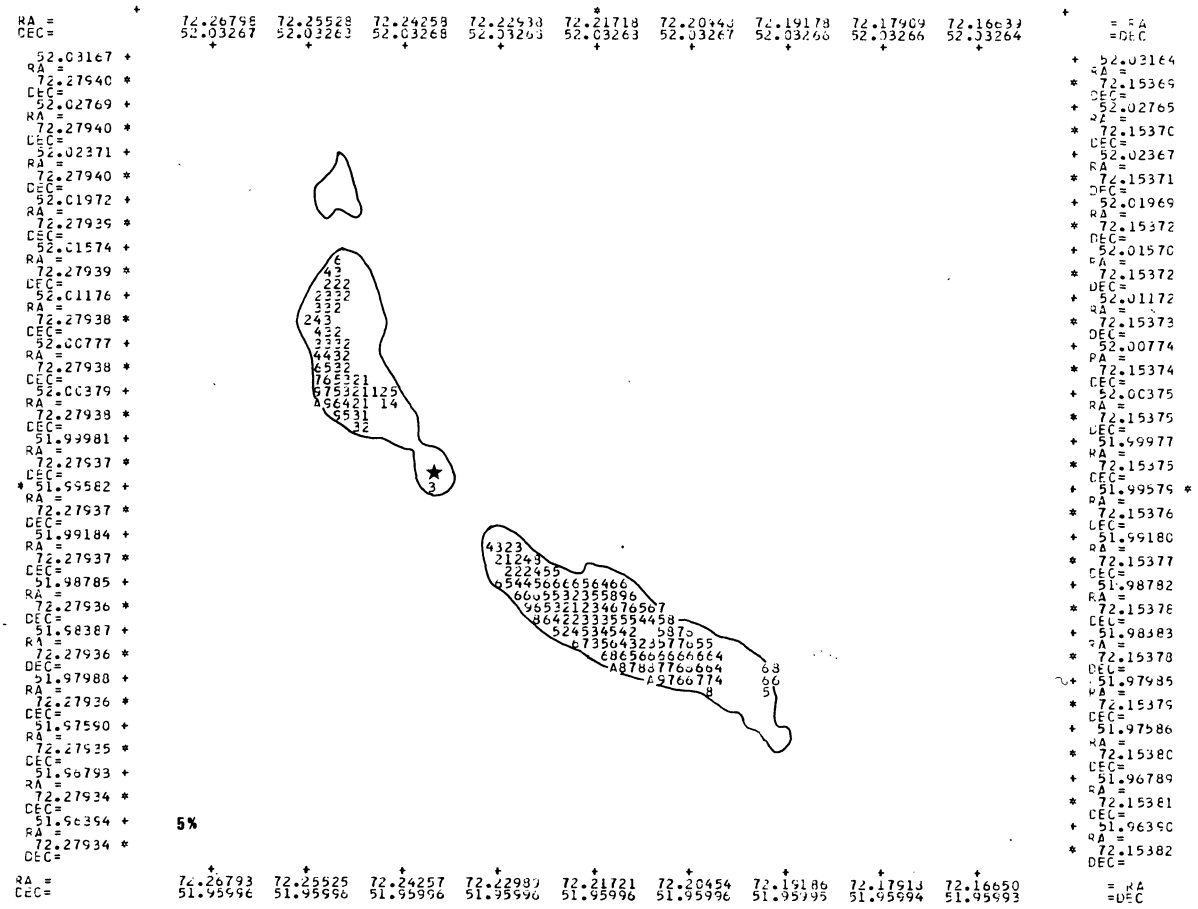

FIGURE 37. — 3C 130, 6 cm %, 4 mJy/beam.

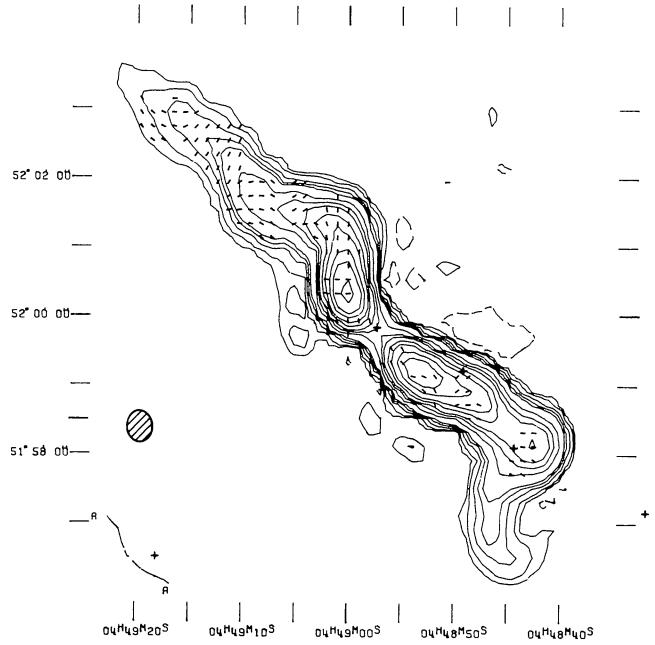

FIGURE 38. — 3C 130, 21 cm I + ϕ ; – 2, 2, 4, 8, 12, 16, 32, 48, 64, 96, 128, 192, 256, 384 mJy/beam.

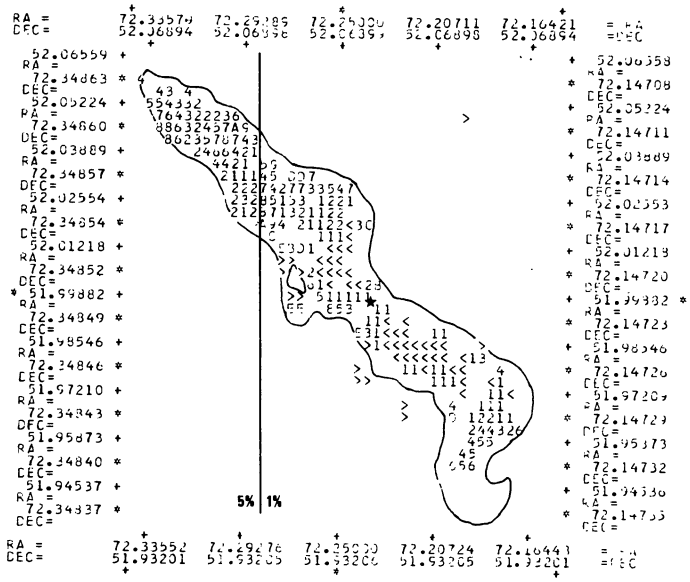

FIGURE 40. — 3C 130, 21 cm % ; 2 mJy/beam.

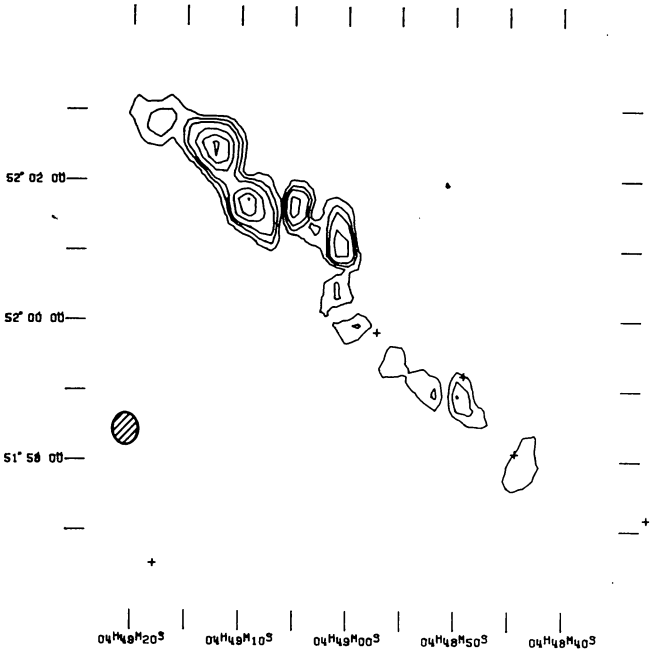

FIGURE 39. — 3C 130, 21 cm P ; 1, 1.5, 2, 3, 4, 5 mJy/beam.

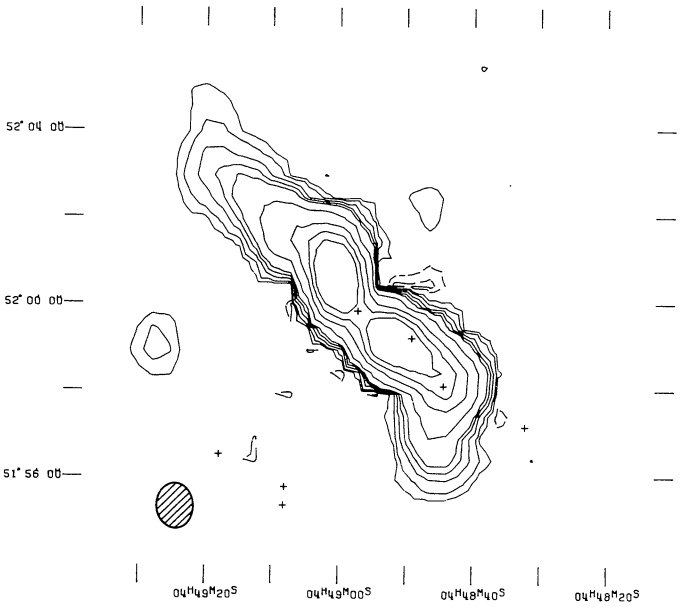

FIGURE 41. — 3C 130, 49 cm I ; – 20, – 10, 10, 20, 40, 60, 80, 160, 320, 480, 640 mJy/beam.

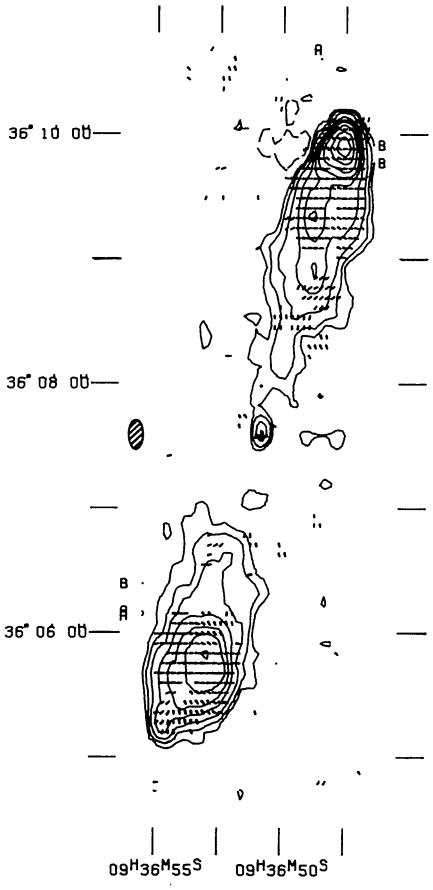

FIGURE 42 (left). — 3C 223, 6 cm I + ϕ ; – 1.25, 1.25, 2.5, 5, 10, 20, 30, 50, 70 mJy/beam.

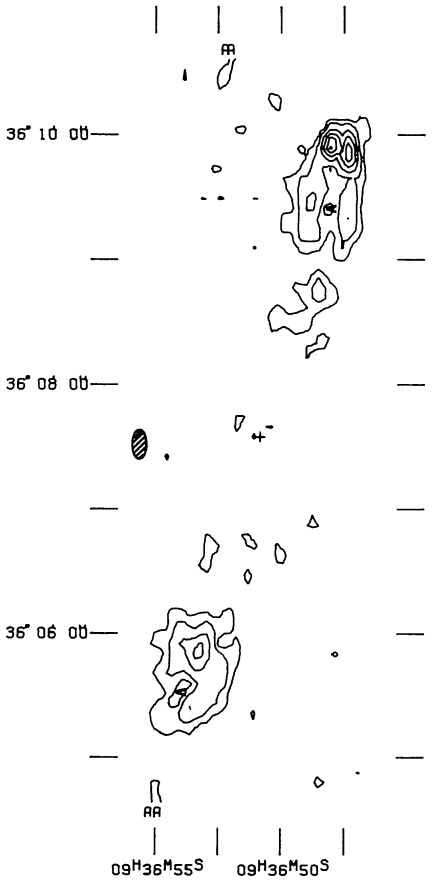

FIGURE 43 (right). — 3C 223, 6 cm P ; 1.25, 2.5, 5, 7.5, 10, 12.5 mJy/beam.

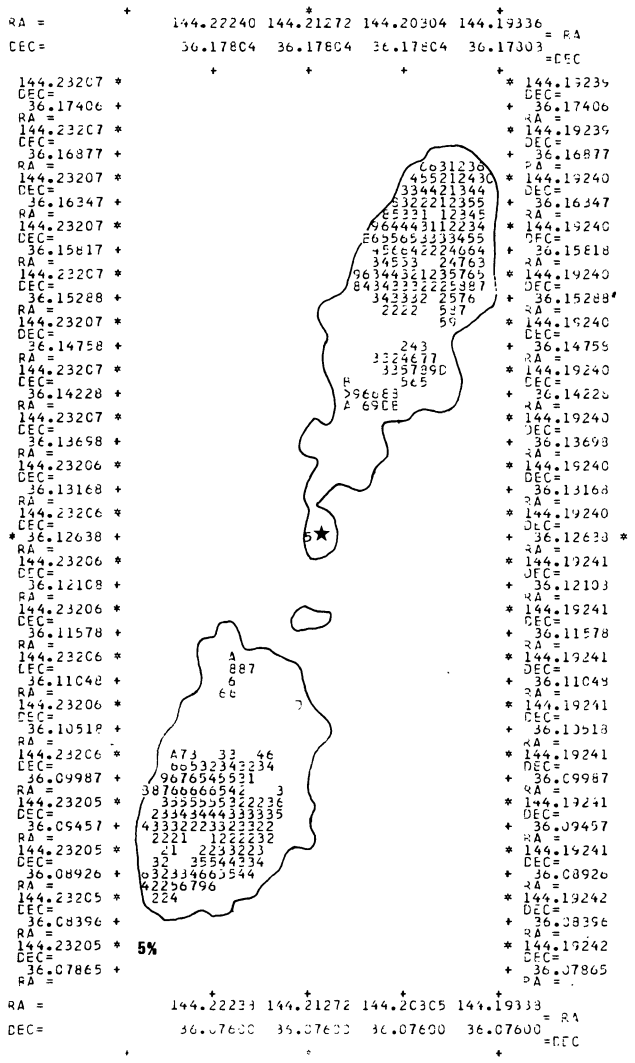

FIGURE 44. — 3C 223, 6 cm % ;
– 20, 20, 40, 80, 160, 320, 480, 640 mJy/beam.

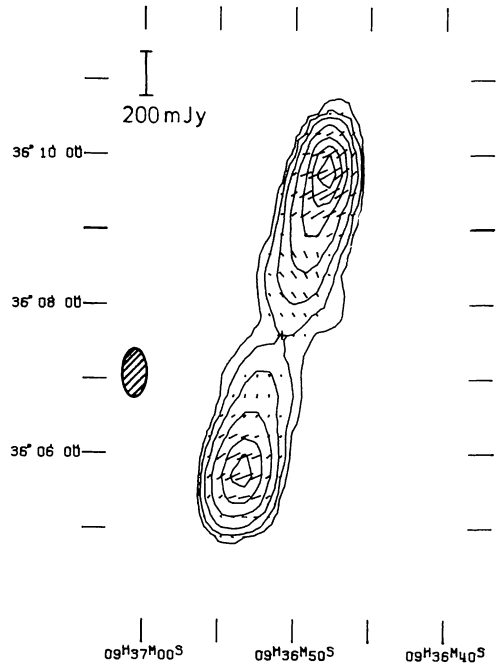

FIGURE 45. — 3C 223, 21 cm I + ϕ ;
– 20, 20, 40, 80, 160, 320, 480, 640 mJy/beam.

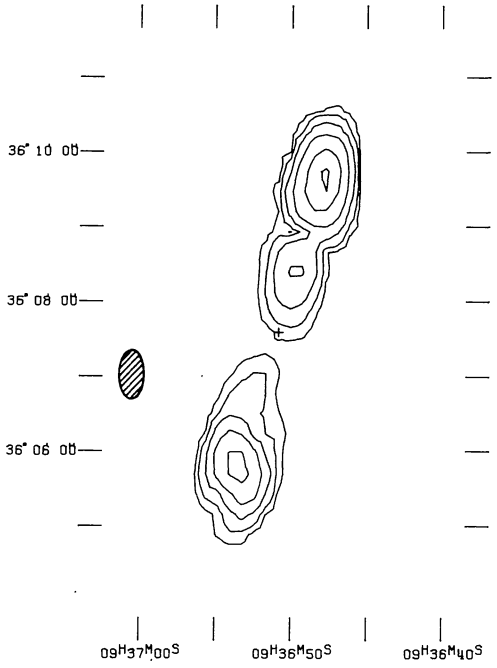

FIGURE 46. — 3C 223, 21 cm P ; 4, 8, 16, 32, 64, 96 mJy/beam.

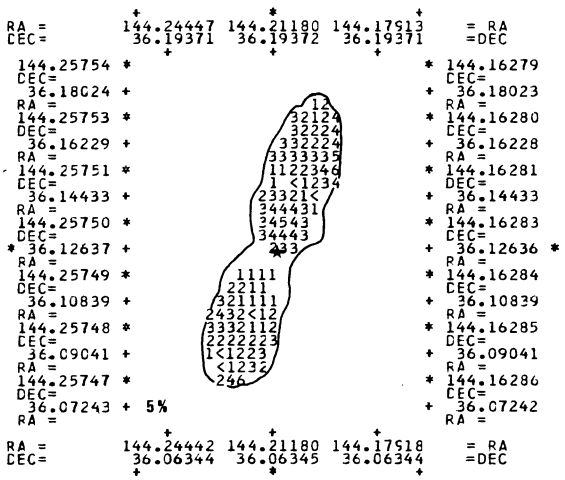

FIGURE 47. — 3C 223, 21 cm % ; 20 mJy/beam.

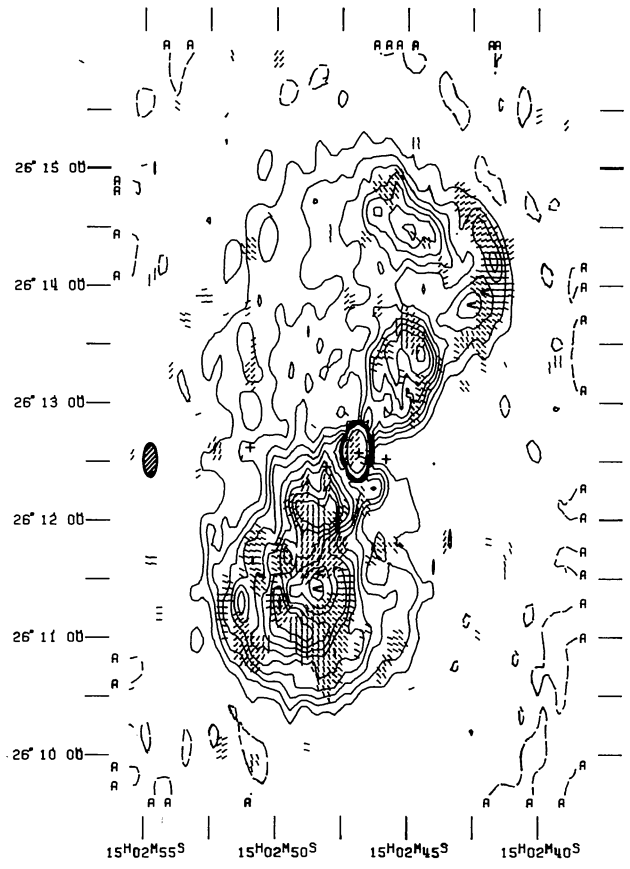

FIGURE 48. — 3C 310, 6 cm I + ϕ ;
– 1, 1, 2, 3, 4, 5, 6, 7, 8, 9, 10, 25 mJy/beam.

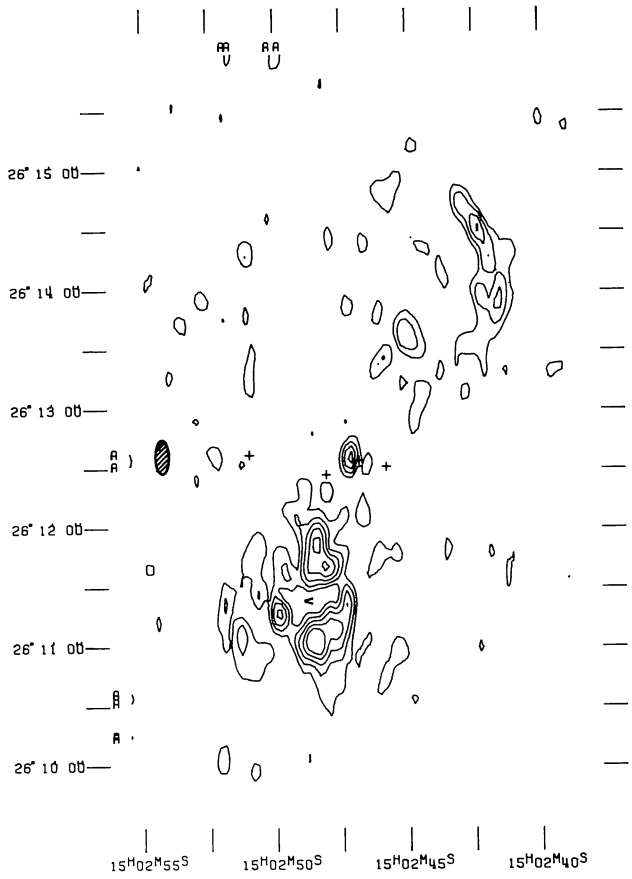

FIGURE 49. — 3C 310, 6 cm P ; 1, 1.5, 2, 2.5, 3 mJy/beam.

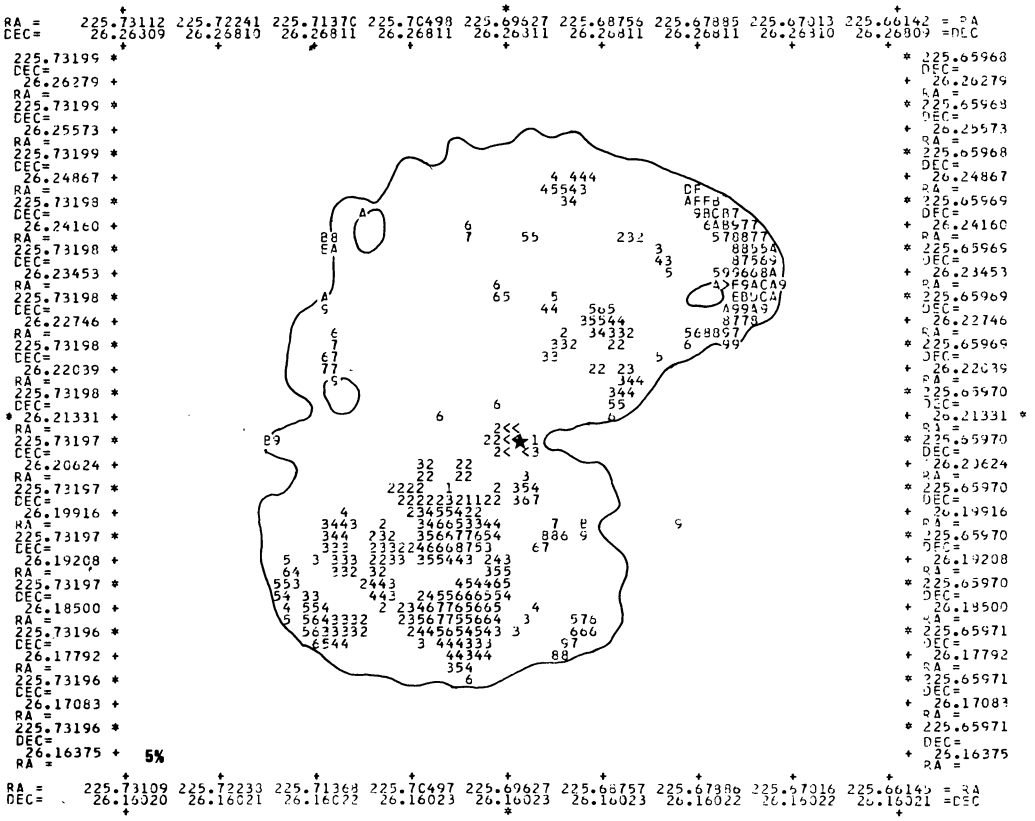

FIGURE 50. — 3C 310, 6 cm %, 1 mJy/beam.

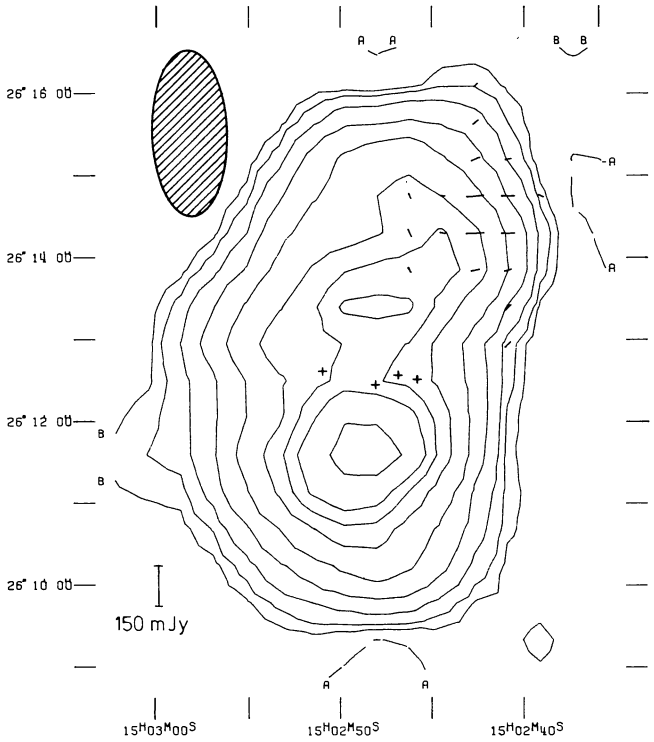

FIGURE 51. — 3C 310, 49 cm I + ϕ ;
– 25, 25, 50, 100, 200, 400, 800, 1200, 1600, 2400 mJy/beam.

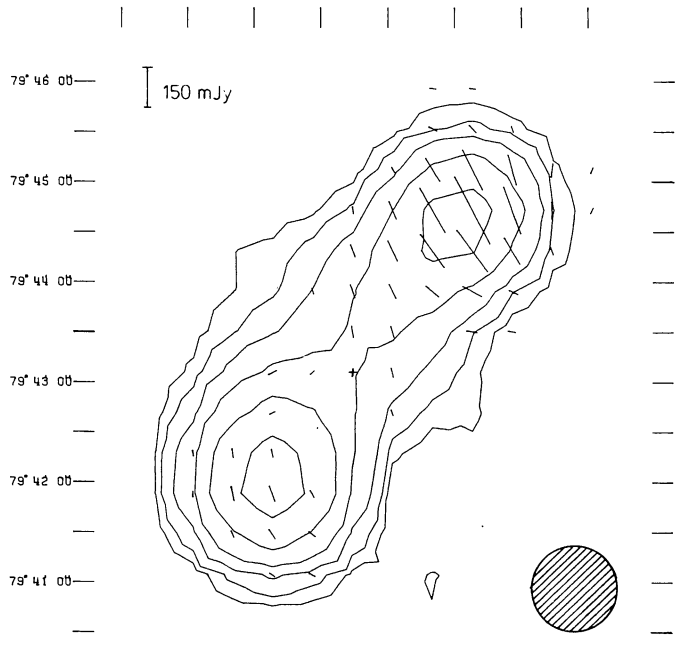

FIGURE 52 (top). — 3C 390.3, 49 cm I + ϕ ;
– 200, 200, 400, 800, 1400, 1600, 3200 mJy/beam.

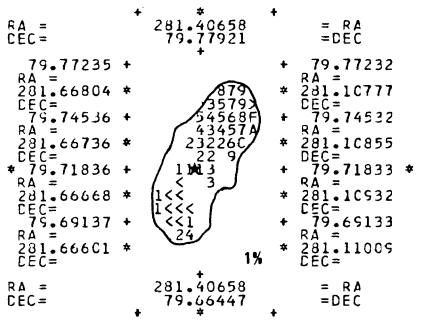

FIGURE 53 (bottom). — 3C 390.3, 49 cm % ; 200 mJy/beam.

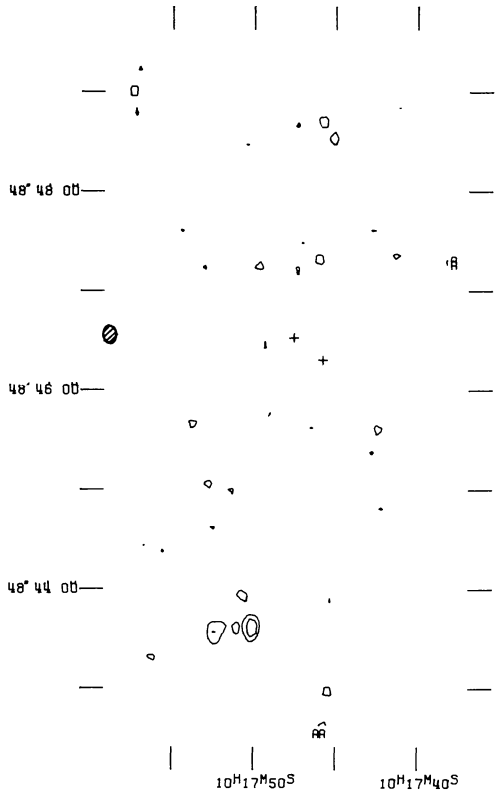

FIGURE 55. — 4C 49.29, 6 cm P ; 1.25, 2.5 mJy/beam.

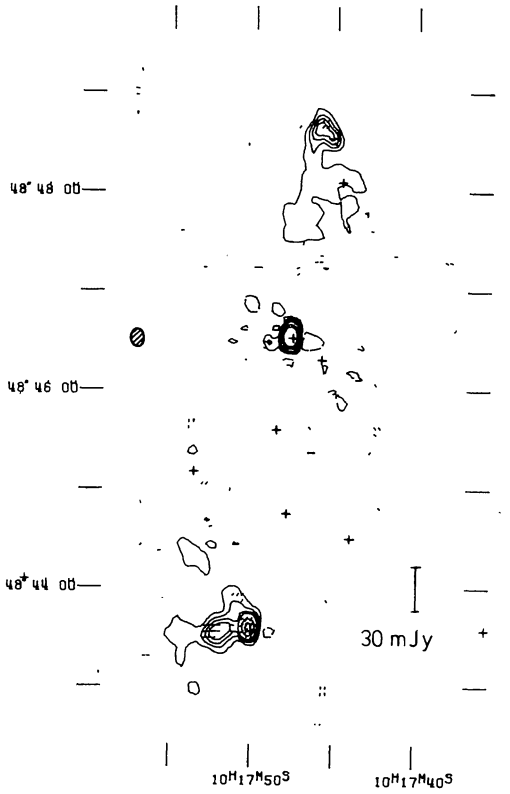

FIGURE 54. — 4C 48.29, 6 cm I + ϕ ; – 2.5, 2.5, 5, 7.5, 10, 20, 30 mJy/beam.

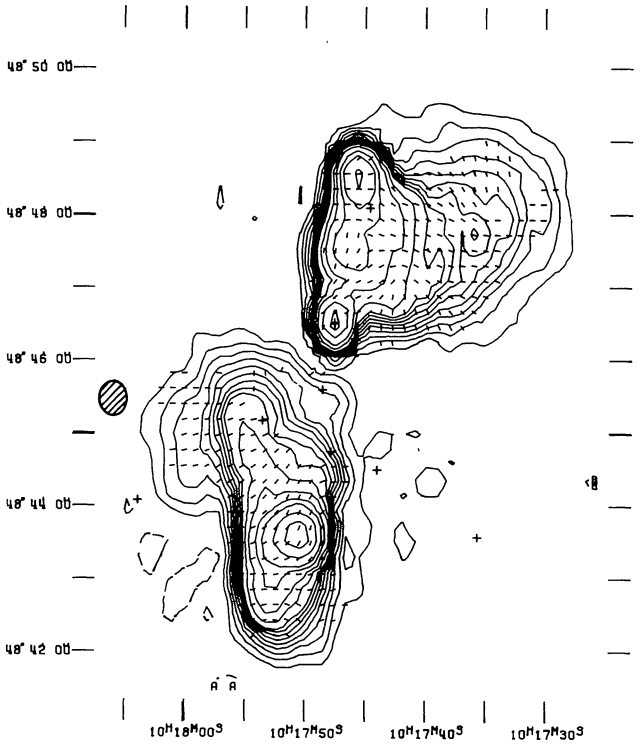

FIGURE 56. — 4C 48.29, 21 cm I + ϕ ; – 2, 2, 4, 6, 8, 10, 12, 14, 16, 18, 24, 32, 48, 64, 100, 150 mJy/beam.

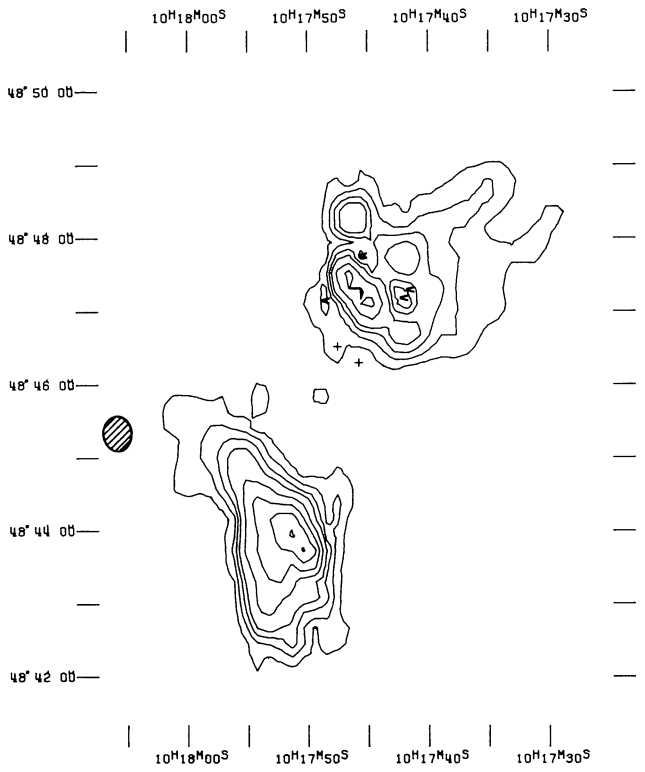

FIGURE 57. — 4C 48.29, 21 cm P ;
1.25, 2.5, 3.75, 5, 7.5, 10, 12.5, 15 mJy/beam.

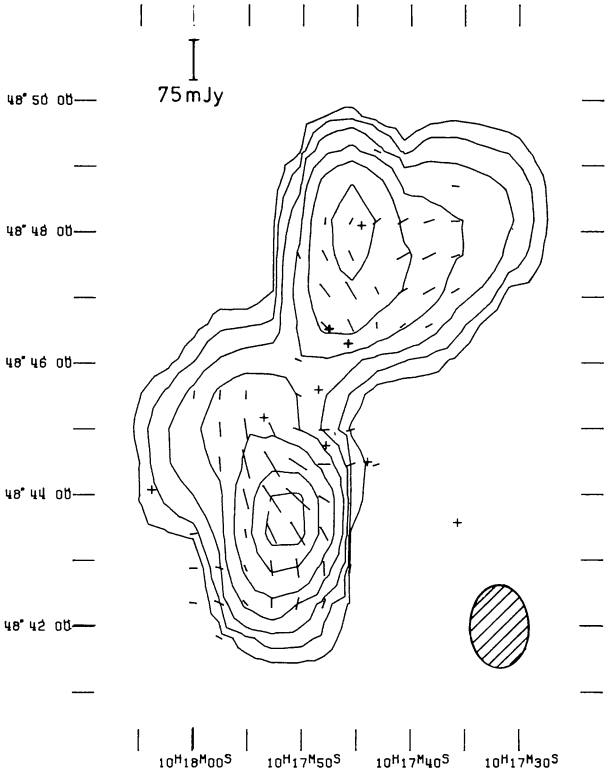

FIGURE 59. — 4C 48.29, 49 cm I + ϕ ;
– 10, 10, 20, 40, 80, 160, 320, 500 mJy/beam.

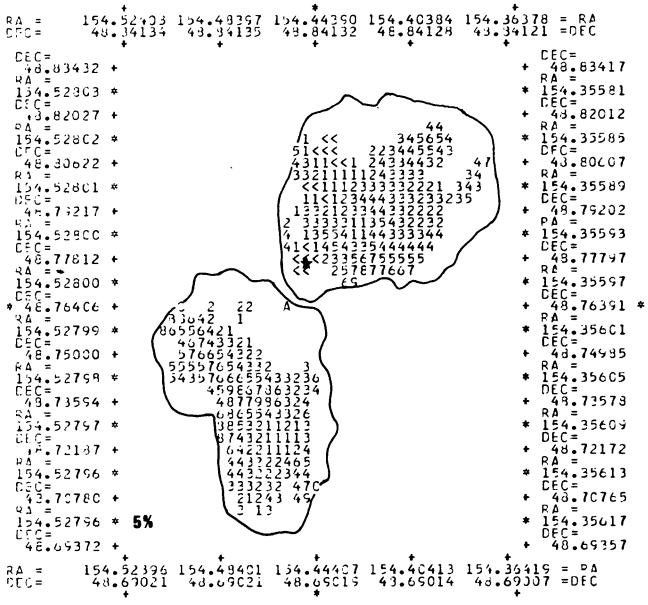

FIGURE 58. — 4C 48.29, 21 cm % ; 2 mJy/beam.

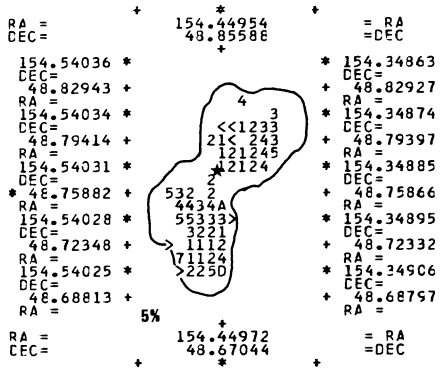

FIGURE 60. — 4C 48.29, 49 cm % ; 10 mJy/beam.